Journal of Hydrology 602 (2021) 126759

Contents lists available at ScienceDirect

Journal of Hydrology

journal homepage: www.elsevier.com/locate/jhydrol

Research papers

Understanding the relationship between rainfall and flood probabilities through combined intensity-duration-frequency analysis

Korbinian Breinl [a,b,1,*], David Lun [a,2], Hannes Müller-Thomy [a,c,3], Günter Blöschl [a,4]

[a] Institute of Hydraulic Engineering and Water Resources Management, Vienna University of Technology, Karlsplatz 13/222, 1040 Wien, Austria
[b] Centre of Natural Hazards and Disaster Science, CNDS, Villavägen 16, 75236 Uppsala, Sweden
[c] Leichtweiß Institute for Hydraulic Engineering and Water Resources, Department of Hydrology, Water Management and Water Protection, Technische Universität Braunschweig, Brunswick, Germany

ARTICLE INFO

This manuscript was handled by Marco Borga, Editor-in-Chief, with the assistance of Francesco Marra, Associate Editor

Keywords:
Rainfall
Floods
Probabilities
Rainfall mechanisms
Catchment characteristics
Elasticity

ABSTRACT

The aim of this paper is to explore how rainfall mechanisms and catchment characteristics shape the relationship between rainfall and flood probabilities. We propose a new approach of comparing intensity-duration-frequency statistics of maximum annual rainfall with those of maximum annual streamflow in order to infer the catchment behavior for runoff extremes. We calibrate parsimonious intensity-duration-frequency scaling models to data from 314 rain gauges and 428 stream gauges in Austria, and analyze the spatial patterns of the resulting distributions and model parameters. Results indicate that rainfall extremes tend to be more variable in the dry lowland catchments dominated by convective rainfall than in the mountainous catchments where annual rainfall is higher and rainfall mechanisms are mainly orographic. Flood frequency curves are always steeper than the corresponding rainfall frequency curves with the exception of glaciated catchments. Based on the proposed approach of combined intensity-duration-frequency statistics we analyze elasticities as the percent change of flood discharge for a 1% change in extreme rainfall through comparing rainfall and flood quantiles. In wet catchments, the elasticities tend to unity, i.e. rainfall and flood frequency curves have similar steepness, due to persistently high soil moisture levels. In dry catchments, elasticities are much higher, implying steeper frequency curves of floods than those of rainfall, which is interpreted in terms of more skewed distributions of event runoff coefficients. While regional differences in the elasticities can be attributed to both dominating regional rainfall mechanisms and regional catchment characteristics, our results suggest that catchment characteristics are the dominating controls. With increasing return period, elasticities tend towards unity, which is consistent with various runoff generation concepts. Our findings may be useful for process-based flood frequency extrapolation and climate impact studies, and further studies are encouraged to explore the tail behavior of elasticities.

1. Introduction

The relationship between rainfall and flood discharge probabilities is important from both practical and theoretical perspectives. The design storm method widely applied in engineering practice consists of estimating a hydrograph with given peak discharge probability from a synthetic rainstorm with the same probability using a rainfall-runoff model (Packman & Kidd, 1980; Pilgrim & Cordery, 1975). Another common procedure that transforms rainfall to flood probabilities is the rational formula, which estimates peak streamflow from a critical rainfall intensity. From a theoretical perspective, the interplay between the statistical behavior of extreme rainfall and catchment processes that produces the flood frequency curve is an interesting topic. For the hypothetical case of rectangular rainstorms of fixed duration, a constant event runoff coefficient and invariant routing, the distribution functions of flood peaks and rainfall intensities are proportional, but for real world

* Corresponding author at: Institute of Hydraulic Engineering and Water Resources Management, Vienna University of Technology, Karlsplatz 13/222, 1040 Wien, Austria.
E-mail address: breinl@hydro.tuwien.ac.at (K. Breinl).
[1] ORCID 0000-0003-0489-4526
[2] ORCID 0000-0003-0382-3371
[3] ORCID 0000-0001-5214-8945
[4] ORCID 0000-0003-2227-8225

https://doi.org/10.1016/j.jhydrol.2021.126759
Received 8 March 2021; Received in revised form 15 July 2021; Accepted 26 July 2021
Available online 2 August 2021

storms and catchments, numerous factors make the flood frequency distribution deviate from that of the rainfall.

The extreme rainfall distribution depends on the climatological situation at the site of interest. Its expected value has been found to be positively correlated with mean annual rainfall in analyses of hourly and daily rain gauge data in different climatic regions (United States, Australia, the British Isles, Japan, India, peninsular Malaysia) (Barbero et al., 2019). In these studies, daily time steps usually exhibited higher correlations than hourly, as the latter were mainly controlled by convection, while the former were also controlled by other mechanisms such as large-scale dynamics and orographic effects that are more relevant at the annual scale. Similarly, positive correlations between daily precipitation extremes and the wet-day mean rainfall have been reported by Benestad et al. (2012) for more than 33,000 rain gauges across the globe.

Single years with exceptional rainfall extremes such as from tropical storms tend to increase the coefficient of variation (CV) of the rainfall distribution and thus the steepness of the rainfall frequency curve (U. S. Weather Bureau, 1958). Depending on the region, these rare extremes can be associated with climate modes such as the El Niño-Southern Oscillation (ENSO) and the Pacific Oscillation (IPO) (Kiem et al., 2003) or with rare interactions of convection-favoring patterns (Piper et al., 2016). Typically, in regions with frequent short-duration convective rainfall events, the CV of annual rainfall maxima is higher and rainfall frequency curves are thus steeper than in more humid regions where rainstorms are longer (Parrett, 1997; Schaefer, 1990). In intensity-duration-frequency statistics, a strong decay with duration reflects peaky rainstorms, suggesting dominance of convective rainfall (e.g. Awadallah, 2015; Breinl et al., 2020; Panthou et al., 2014; Sane et al., 2018). Higher expected values of the rainfall distribution and larger CVs may lead to higher and steeper flood frequency curves, everything else being equal (Merz & Blöschl, 2003; Smith et al., 2011; Villarini & Smith, 2010).

Another relevant factor controlling the flood frequency curve is antecedent catchment wetness (Berghuijs et al., 2016; Komma et al., 2007; Slater & Villarini, 2016). In wet catchments, storage capacities tend to be lower and event runoff coefficients tend to be higher, thus increasing flood discharges of a given probability relative to dry catchments (Borga et al., 2007; Vivoni et al., 2007). More specifically, it has been suggested that the distribution of event runoff coefficients influences the steepness of the flood frequency curve: In arid catchments where infiltration excess dominates, the event runoff coefficients are mainly random as opposed to more humid catchments, where runoff coefficients are less variable (Merz & Blöschl, 2009b; Sivapalan et al., 2005). Infiltration excess runoff is typical of convective rainfall regions with large CVs of rainfall extremes (Keefer et al., 2016), so the flood frequency curves are typically steeper than in more humid catchments dominated by synoptic rainfall (Basso et al., 2016; Franchini et al., 2005; Guo et al., 2014; Hashemi et al., 2000; Viglione et al., 2009). Steeper flood frequency curves can also be a consequence of the spatial distribution of the rainfall, as rare extreme flood peaks can occur if locally high rainfall intensities match locally high soil moisture (Bell & Moore, 2000; Zhu et al., 2018). Additionally, a steep flood frequency curve can be the result of rainfall exceeding a threshold of soil storage capacity (Rogger et al., 2012), a threshold of epikarst storage in karstic environment (Li et al., 2017) or other threshold processes of runoff generation (Struthers & Sivapalan, 2007; Zehe & Sivapalan, 2009).

Runoff routing may also impact the flood frequency curve (Blöschl & Sivapalan, 1997; Norbiato et al., 2008), as the largest floods are produced when storm duration matches the response time (Viglione & Blöschl, 2009). A faster runoff response with increasing event magnitude, as it often occurs due to a higher relevance of surface and near surface flow paths and greater surface flow depths, will be reflected in an increasingly steeper flood frequency curve with return period (Rogger et al., 2012).

One way of quantifying the relationship between rainfall and flood probabilities is the concept of elasticity, which is defined as the relative change in streamflow divided by the relative change in precipitation (e.g. Sankarasubramanian et al., 2001). While in the past the elasticity concept in hydrology has mainly been applied to annual rainfall and streamflow, we believe it has also potential for rainfall and streamflow extremes. If the flood frequency curve is proportional to the rainfall frequency curve, the elasticity is unity. If the flood frequency curve is steeper than the rainfall frequency curve, elasticity is greater than unity. Studies on annual rainfall and streamflow found that streamflow is most sensitive to rainfall change in dry catchments due to the nonlinearity in the rainfall-runoff process (e.g. Chiew, 2006; Sankarasubramanian et al., 2001; Tang et al., 2019; Yang & Yang, 2011). For extreme rainfall and floods, there seems to similarly exist a stronger sensitivity in dry catchments. For example, the data of Paquet et al. (2013) suggest that a 1% increase of an extreme 72hr rainfall (300 mm) produced a 2.6%, 2.0% and 1.5% increase in extreme runoff for dry, intermediate and wet conditions (estimated from Fig. 16 of Paquet et al. (2013)). However, to the best of our knowledge we are not aware of data-based regional analyses that have explored flood sensitivities to extreme rainfall.

Most of the above studies have analyzed the rainfall-to-flood probability transformation by a model-based derived flood frequency concept (e.g. Sivapalan et al., 2005; Viglione & Blöschl, 2009; Viglione et al., 2009; Zhu et al., 2018). Studies on the rainfall elasticity of streamflow have similarly been model-based (e.g. Chiew, 2006; Tang et al., 2019) or have focused on annual streamflow rather than extremes (e.g. Sankarasubramanian et al., 2001; Yang & Yang, 2011). While model-based approaches are able to isolate individual factors well, it is difficult to ascertain model validity. Real world processes may deviate from those assumed in the models as the consequence of the coevolution of climate and landscape processes (Perdigão and Blöschl, 2014). On the other hand, an analysis of a large data set of rainfall and runoff observations may be able to shed light on the more complex real-world relationship between rainfall and flood probabilities, including different rainfall mechanisms and non-linear runoff generation processes as a function of soil type and geology.

The aim of this paper therefore is to explore how rainfall mechanisms and catchment characteristics shape the relationship between rainfall and flood probabilities based on comprehensive runoff and rainfall observations. To this end we propose a new approach of comparing intensity-duration-frequency statistics of maximum annual rainfall with those of maximum annual streamflow.

The analysis is based on a high quality data set of 314 rain gauges and 428 runoff gauges in Austria. In order to identify the effects of individual processes on the probability relationship we adopt the concept of comparative hydrology, contrasting catchments with different rainfall and runoff generation processes (Blöschl et al., 2013). Rather than evaluating individual events we estimate intensity-duration-frequency statistics for both rainfall and streamflow and compare them for equivalent return periods, evaluating the elasticity of floods to rainfall extremes. In order to minimize the effects of snow melt, we focus on the summer season when most of the floods in Austria occur (Gaál et al., 2012).

The relevance of the study is twofold. First, the elasticities explored here enable more informed extrapolations to larger than observed floods using rainfall statistics (e.g. Goel et al., 2000). Second, the elasticities may also shed light on the impact of climate change on flood through changing rainfall extremes. The study may also underpin a more informed application of methods for estimating design floods. The research addresses two of the 23 Unsolved Problems in Hydrology (UPH), i.e. “5: What causes spatial heterogeneity and homogeneity in runoff, evaporation, subsurface water and material fluxes” and “10: Why are runoff extremes in some catchments more sensitive to land-use/cover and geomorphic change than in others?” (Blöschl et al., 2019).

The paper is structured as follows: section 2 provides an overview of the study region and data. The methods section 3 introduces the intensity-duration-frequency models for both extreme rainfall and

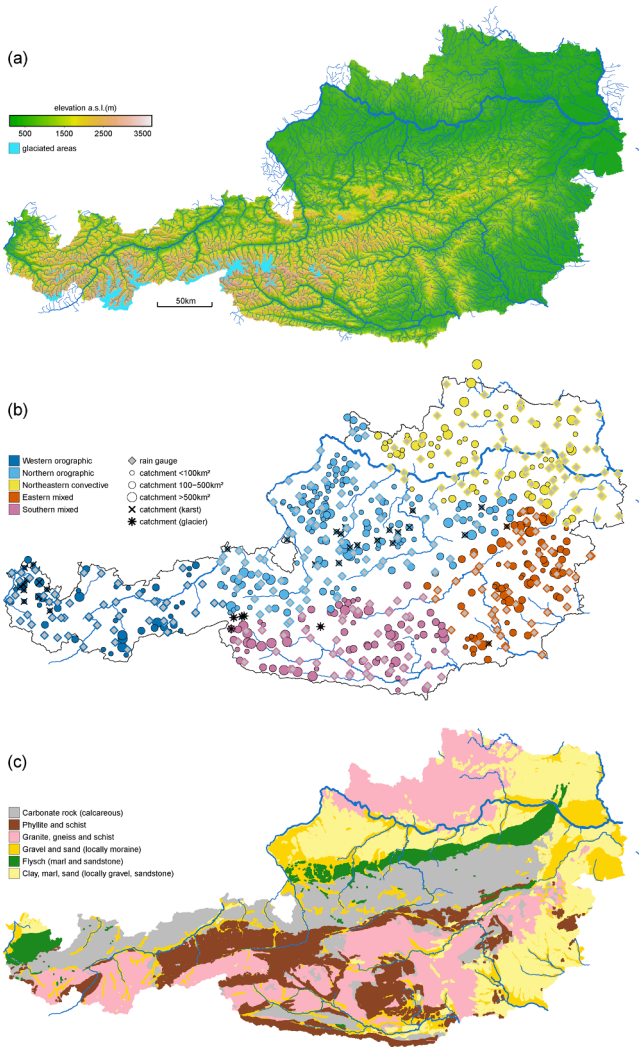

Fig. 1. (a) Topography of Austria with river network and glaciated areas. (b) Five rainfall regions representing different dominating rainfall mechanisms, rain gauge network and catchment centroids of gauged catchments. Catchments impacted by karst are marked with crosses, those by glaciers with asterisks. (c) Geology of Austria.

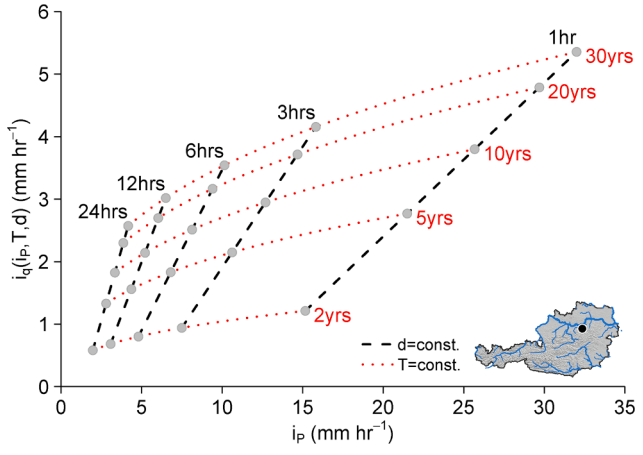

Fig. 2. Relationship between flood i_q and rainfall i_P intensities for an example catchment ("Melk", catchment area 95.2 km^2). Dashed black lines indicate constant durations d, dotted red lines indicate constant return periods T.

streamflow and the analytical solution of the extreme rainfall elasticity to floods, which we use to compare the rainfall and streamflow distributions. In the results section 4, we explain the spatial patterns of the rainfall and streamflow characteristics as well as the elasticities by rainfall mechanisms, topography, soils, geology and climate variables. The paper finishes with a discussion and conclusions.

2. Study region and data

The study is set in Austria (84,000 km^2). In the North, East and South East elevations are below 200 m above sea level, while the highest Alpine summits reach over 3,500 m (Fig. 1a). Mean annual rainfall ranges from less than 400 mm yr^{-1} in the East to more than 3000 mm yr^{-1} in the West.

We used hourly streamflow data from stream gauges in Austria for the period 1976–2015 (June to August), with a mean length of 36 years (maximum of 40 years, minimum of 21 years). Time series of catchments strongly influenced by hydraulic infrastructure were excluded, which resulted in 428 catchments with areas ranging from 3.9 km^2 to 4,792 km^2 and a median of 125 km^2 (Fig. 1b). We also used hourly rainfall observations from 314 Austrian rain gauges for the period 1950–2016 (June to August) with a mean length of 20 years (maximum of 43 years, minimum of 10 years) (Fig. 1b). Catchments impacted by Karst springs were identified based on a visual comparison with hydrogeological maps.

Rainfall and flood mechanism vary considerably within the study region. In general, convective rainfall and flash floods are most frequent in the lowlands, identifiable by a higher frequency of hailstorms, severe wind gusts and tornados in these regions (Fig. A1, Dotzek et al. (2009) and Merz and Blöschl (2003)), while short-rain and long-rain floods from orographic rainfall are most frequent along the Alpine ridge (Merz & Blöschl, 2003), aligned with longer wet spells and shorter dry spells along the Alpine ridge compared to the lowlands (Fig. A2). Throughout Austria, floods are more frequent in the summer than in the winter (Merz & Blöschl, 2003).

To investigate the regional differences, rain gauges and catchments were grouped into five regions based on the previous rainfall-based classifications by Matulla et al. (2003), Seibert et al. (2007) and Breinl et al. (2020) (Fig. 1b). We chose a rainfall-based classification in order to better understand regionally dominant factors in runoff formation. (i) The "Western orographic" region is dominated by orographic rainfall due to airflows from Western, NNW and NW directions. Long-rain floods are most frequent and the highest catchments are affected by glacier melt (Gaál et al., 2012). (ii) In the "Northern orographic" region heavy rainfall is mainly caused by NNW, NW and West airflows from the Atlantic (Seibert et al., 2007) producing long-rain floods. (iii) In the "Northeastern convective" region in the northern lowlands of Austria, frequent convective rainstorms produce flash floods, and Westerly flows produce long-rain floods. The latter include "Vb" weather situations, where moist air from the Adriatic sea is advected causing heavy rainfall (Seibert et al., 2007). (iv) The "Eastern mixed" region is influenced by convective activity, partly due to the hilly terrain, which increases the instability of the boundary layer (Merz & Blöschl, 2003) leading to frequent flash floods, and hail storms. (v) The "Southern mixed" region is similarly influenced by convective activity, sometimes associated with weak gradient situations, and rainfall extremes can also be related to the advection of humid air from the Mediterranean (Gaál et al., 2012; Seibert et al., 2007).

Flood response is also influenced by geology (Fig. 1c). The Flysch zone along the Northern fringe of the Alps is characterized by low subsurface permeability and thus surface or near surface flow paths, leading to flashy response. Similarly, shallow soils and efficient drainage networks in the Southeast lead to short response times (Gaál et al., 2012). On the other hand, in the Phyllite region in the South, deeply weathered metamorphic rock is associated with deep flow paths and slow flood response (Gaál et al., 2012). The latter is also typical for the

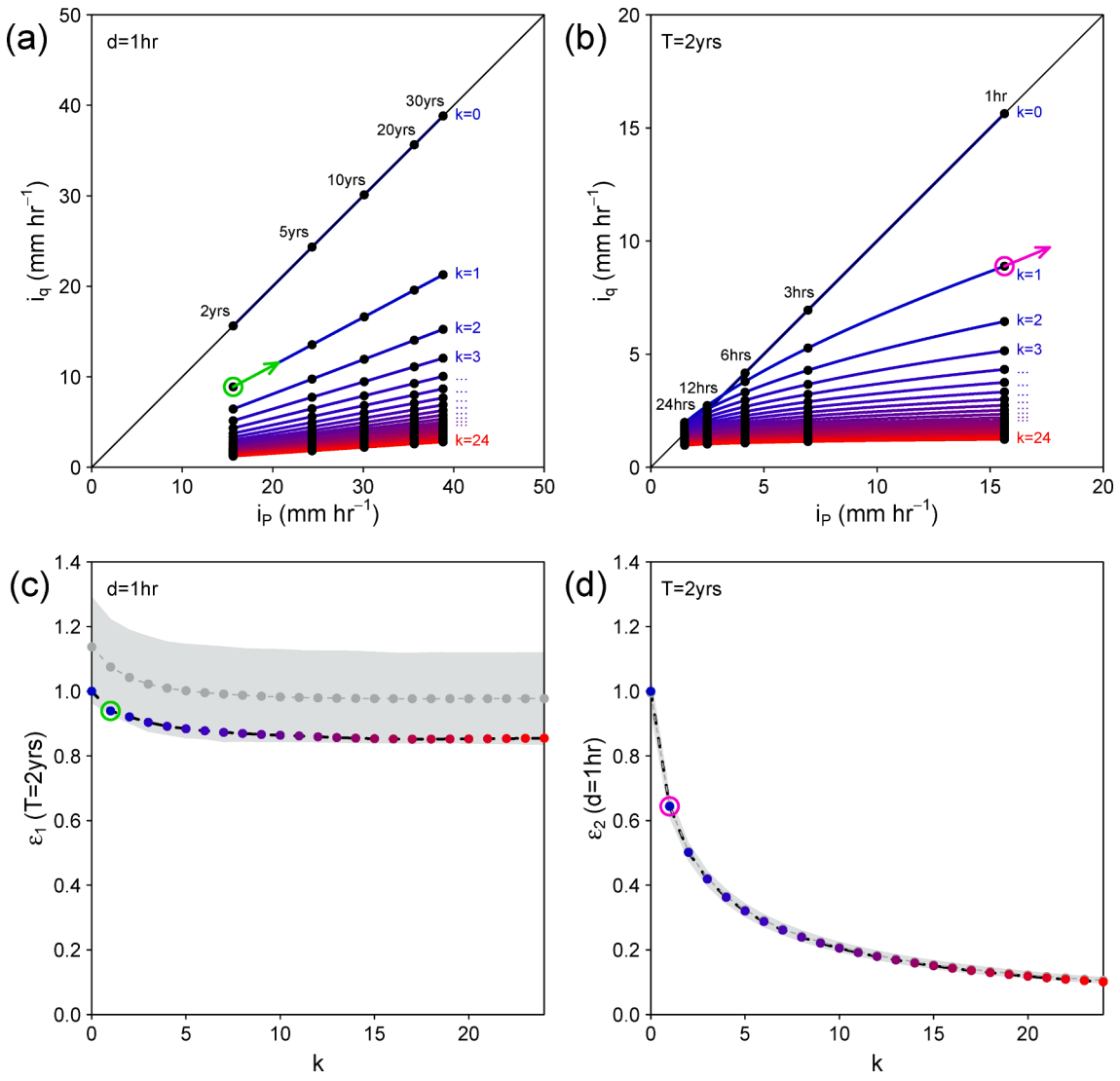

Fig. 3. Relationship between flood i_q and rainfall i_P intensities (a,b) and related elasticities (c,d) estimated from observed rainfall time series at the rain gauge "Hohe Warte" and a linear reservoir over a range of storage coefficients k. (a) Relationship for d = 1hr and (b) T = 2yrs. (c) Elasticities ε_1 assuming d = 1hr is constant at a return period of T = 2yrs. Blue to red points correspond to varying k and a runoff coefficient rc = 1; Gray points correspond to the median of 100 simulations for each k with rc varying randomly according to a beta distribution with parameters $\alpha = 2$ and $\beta = 5$, i.e. a mean of about 0.29. The shaded area corresponds to the 5th and 95th percentiles of the simulations. (d) Elasticities ε_2 assuming T = 2yrs is constant at a duration of d = 1hr. Blue to red points correspond to varying k and rc = 1; Gray line and shaded area correspond to randomly varying rc as in (c).

catchments dominated by gravel and sand aquifers, for example in the Northwest and East (Gaál et al., 2012).

3. Methods

Studies that explain the generating mechanisms of floods in a probabilistic context usually compare the flood frequency curve with event-based rainfall and catchment drivers (e.g. Arnaud & Lavabre, 2002; Rahman et al., 2002; Stein et al., 2021). In this paper, however, we have chosen the flood-duration-frequency (QDF) curve (e.g. Cunderlik & Ouarda, 2006, 2007; Javelle et al., 2003; Javelle et al., 2002) as a starting point instead, in order to approach the problem in a more general way. A QDF curve is composed of extreme value distributions of streamflow for different aggregation intervals. For example, one identifies the maximum hourly streamflow (i.e. streamflow averaged over one hour) in every year and constructs a frequency distribution from that. In a similar way frequency distributions are constructed for other aggregation intervals, thus obtaining a family of curves for a particular catchment. In the limit of the aggregation interval of d = 0, the QDF curve is equivalent to the traditional flood frequency curve. The QDF curve can therefore be considered an extension of the latter, as it not only contains information on the peak but also on the shape of the hydrographs. For example, if the 1hr and 12hrs distributions are similar, hydrographs are subdued, while much larger streamflow for 1hr than for 12hrs points towards peaky hydrographs.

The idea of QDF curves is similar to that of intensity-duration-frequency (IDF) curves of rainfall (e.g. Sivapalan & Blöschl, 1998), which are estimated in an analogous way. The IDF curves are a fingerprint of the extreme rainfall regime in terms of increasing rainfall intensities with increasing return period and decreasing duration. A steep dependence of rainfall intensity on the return period (i.e. representing a large variability between years) may indicate the dominance of convective over frontal rainfall mechanisms (Parrett, 1997; Schaefer, 1990).

Because of the similarity of the IDF and QDF concepts, their comparison is straightforward. In fact, for a hypothetical rainfall-runoff transformation where all rainfall becomes runoff (event runoff coefficient $r_c = 1$) and an infinitely fast runoff concentration (time of

Table 1
Model parameters and spatial process indicators used in each catchment in the correlation analysis.

Information	Abbreviation	Description	Unit
Model parameters (streamflow)	λ_q	Scale parameter (proportional to the standard deviation of the streamflow extremes for a given duration)	mm
	ψ_q	Location parameter (magnitude of the streamflow extremes, ceteris paribus)	–
	η_q	Scaling parameter (change of intensity with duration, indicator for flashiness of response)	–
Model parameters (rainfall) – interpolated from rain gauge locations to catchment centroids	λ_P	Scale parameter (proportional to the standard deviation of the rainfall extremes for a given duration)	mm
	ψ_P	Location parameter (magnitude of the rainfall extremes, ceteris paribus)	–
	η_P	Scaling parameter (change of intensity with duration, indicator for convective activity)	–
Topographic indices	area	Area of catchment	km^2
	elevation	Mean catchment elevation (m.a.s.l.)	m
	slope	Mean topographic slope	%
	network density	Density of river network	m/km^2
Soil attributes	soil depth	Depth of soils	m
	bulk density	Bulk density of soils	kg/m^3
	Fluvisol, Lithosol, Rendzina, Phaeozem, Chernosem, Cambisol, Luvisol, Podsol, Histosol	Fraction of area of Fluvisol, Lithosol, Rendzina, Phaeozem, Chernosem, Cambisol, Luvisol, Podsol and Histosol in catchment	%
Geology	Carbonate rock, Phylitte, Granite, Gravel and sand, Flysch, Clay	Fraction of area of Carbonate rock, Phylitte, Granite, Gravel and sand, Flysch and Clay in the catchment	%
Climate indicators	MAP	Long-term mean annual rainfall	mm $year^{-1}$
	MSP	Long-term mean seasonal summer rainfall June/July/August	mm $season^{-1}$
Event runoff coefficients	–	Event runoff coefficients for the summer season June/July/August	

concentration $t_c = 0$), IDF and QDF curves are identical. In reality, the event runoff coefficient is smaller than 1 and the time of concentration is greater 0, and therefore the QDF curve will differ from the corresponding IDF curve. The deviations will depend on runoff generation (event runoff coefficients and their distribution), runoff concentration (times of concentration and any nonlinearities that may be present) as well as the rainfall characteristics. For example, in catchments with short response times, short intense rainstorms will lead to particularly high flood peaks and the QDF curve will therefore mainly reflect the short durations of the IDF curve, while the longer durations are less relevant (see Fig. 7a in Viglione & Blöschl (2009)).

In order to shed light on the similarities between the QDF curves and their associated IDF curves we fit IDF and QDF models independently to observations of rainfall and streamflow data, respectively, and compare them in a second step.

3.1. Probability models for rainfall and streamflow extremes

For representing extreme rainfall, we adopt the model of Koutsoyiannis et al. (1998):

$$i_P = \frac{a(T_P)}{b(d_P)} \tag{1}$$

where i_P is the maximum annual rainfall intensity (mm hr^{-1}) of duration d_P at a station, and a and b are terms that only depend on the return period T_P and the duration d_P, respectively. The denominator is parameterized by a scaling relationship with duration, while the enumerator is represented by a Gumbel distribution, which was found to represent the Austrian rainfall data well (Breinl et al., 2020). The IDF model (quantile function) is thus defined as (Koutsoyiannis et al., 1998):

$$i_P = \frac{a(T_P)}{b(d_P)} = \lambda_P \frac{\psi_P - \ln\left[-\ln\left(1-\frac{1}{T_P}\right)\right]}{(d_P)^{\eta_P}} \tag{2}$$
$$\text{with } \lambda_P > 0; T_P > 1; d_P \geq 1\text{hr}; 0 < \eta_P < 1$$

with the location parameter ψ_P, the scale parameter λ_P and the scaling parameter η_P.

In order to facilitate the comparison with rainfall, we use an analogous model for streamflow, i.e., the QDF relationship is represented by

$$i_q = \frac{a(T_q)}{b(d_q)} = \lambda_q \frac{\psi_q - \ln\left[-\ln\left(1-\frac{1}{T_q}\right)\right]}{(d_q)^{\eta_q}} \tag{3}$$
$$\text{with } \lambda_q > 0; T_q > 1; d_q \geq 1\text{hr}; 0 < \eta_q < 1$$

where i_q is the maximum annual specific streamflow (mm hr^{-1}). A log-likelihood ratio test (e.g. Smith, 1992) on the Austrian data confirmed that the Gumbel distribution is preferable over a GEV distribution for the majority of gauges.

The parameters of the IDF and QDF models can be interpreted as follows: The scale parameters λ_P and λ_q, for a given duration, are directly proportional to the standard deviations σ_P and σ_q of the random variables:

$$\sigma_P = \lambda_P d_P^{-\eta_P} \frac{\pi}{\sqrt{6}};\ \sigma_q = \lambda_q d_q^{-\eta_q} \frac{\pi}{\sqrt{6}} \tag{4}$$

The location parameters ψ_P and ψ_q describe the shift of the distributions, i.e. a higher location parameter implies higher rainfall or streamflow extremes, ceteris paribus. The average magnitudes of rainfall and streamflow extremes are defined by the expected values μ_P and μ_q of the random variables

$$\mu_P = \lambda_P d_P^{-\eta_P}(0.5772 + \psi_P);$$
$$\mu_q = \lambda_q d_q^{-\eta_q}(0.5772 + \psi_q) \tag{5}$$

and thus depend on the duration, scale and scaling parameters.

The scaling parameters η_P and η_q quantify the decay of intensity with increasing duration. At stations where extreme rainstorms are short (e.g. due to convective rainfall), η_P tends to be high, reflecting a strong decay, whereas at stations where extreme rainstorms are longer (e.g. due to frontal rainfall) η_P tends to be lower (Llasat, 2001; Mohymont et al., 2004; Panthou et al., 2014). For example, Mohymont et al. (2004) and Panthou et al. (2014) who used a similar scaling model found high values of η_P in zones of high convective activity. For the case of streamflow, the scaling parameter η_q reflects the flashiness of catchment response, i.e. slim hydrographs are associated with larger values of η_q

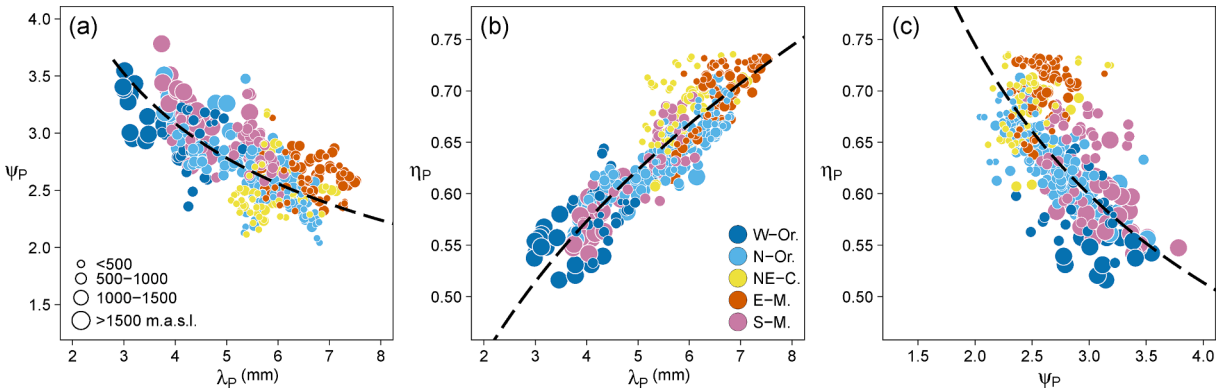

Fig. 4. Interdependencies of the calibrated (interpolated) model parameters of the rainfall model λ_P (scale parameter representing rainfall variability), ψ_P (location parameter representing rainfall magnitude, ceteris paribus) and η_P (scaling parameter representing the dependence on duration). Point sizes relate to catchment centroid elevations and colors indicate rainfall regions in Austria (Fig. 1b).

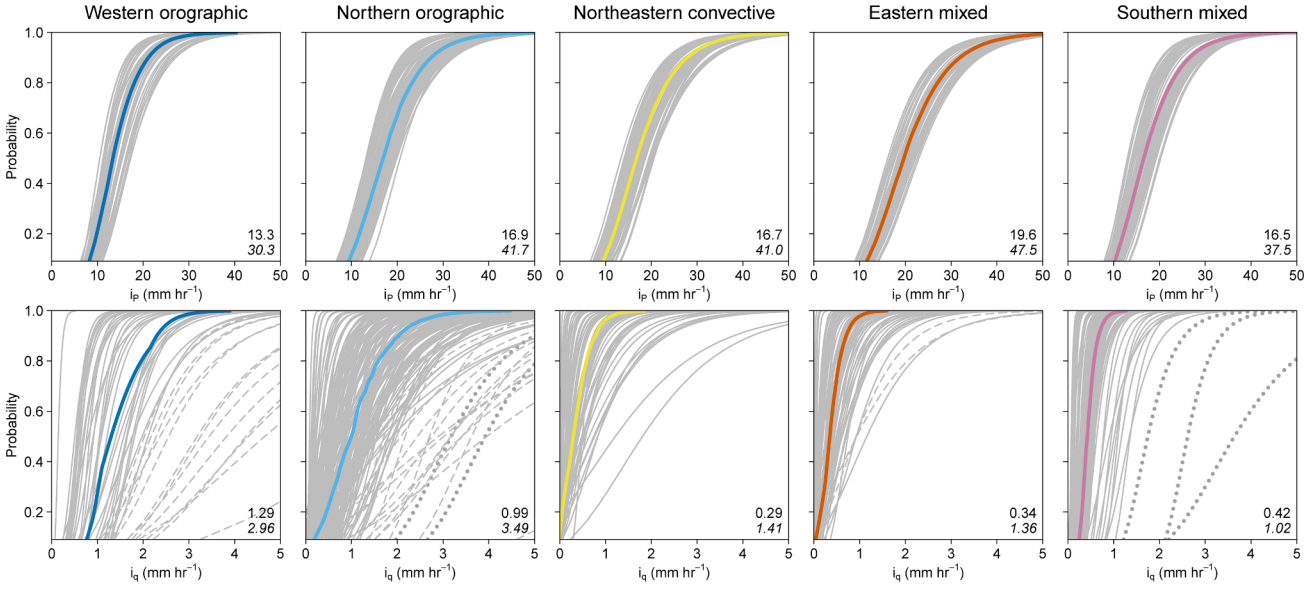

Fig. 5. Cumulative distribution functions of rainfall i_P (upper row) and specific streamflow i_q (bottom row) extremes with a duration of 1hr in the five rainfall regions. Colored lines represent the median CDFs in each region, numbers in the plot area refer to the 5% and 99% quantiles (italic) of the median. Dashed and dotted grey lines represent catchments impacted by Karst springs and glaciers, respectively (see Fig. 1b).

than more subdued hydrographs.

The CVs of i_P and i_q are expressed as:

$$CV_P = \frac{\pi}{\sqrt{6}\ (0.5772 + \psi_P)}; \qquad CV_q = \frac{\pi}{\sqrt{6}\ (0.5772 + \psi_q)} \tag{6}$$

This means, the CVs (Equation (6)) only depend on the respective location parameters ψ_P and ψ_q. This is a consequence of the form of the scaling models (Equations (2) and (3)).

Annual maximum intensities of rainfall were extracted from the hourly rainfall series for the period June-August using a moving window of five durations $(1\text{hr}, 3\text{hrs}, 6\text{hrs}, 12\text{hrs}, 24\text{hrs})$. Empirical return periods were assigned to each annual maximum for each duration using Gringorten plotting positions (Koutsoyiannis et al., 1998). All parameters of the rainfall model were then fitted in one step by minimizing the logarithmized least squares deviation between the intensities of the observation and the model using the derivative-free optimization algorithm of Powell (2009). The mean absolute percentage difference (averaged over all gauges and durations) between the fitted intensities and the intensities obtained by separately fitting Gumbel distributions with maximum likelihood was 3.0% (2.8% for d = 1hr, 4.1% for d = 24hrs) for T = 2yrs, and 8.5% (12.7% for d = 1hr, 10.4% for d = 24hrs) for T = 100yrs. The streamflow model was fitted in an analogous way and the corresponding goodness of fit figures were 7.0% (5.1% for d = 1hr, 7.0% for d = 24hrs) and 8.5% (9.6% for d = 1hr, 11.7% for d = 24hrs), respectively.

3.2. Combined rainfall-flood relationship

The IDF and QDF curves for a given catchment can be compared in different ways. Here, we chose to compare streamflow quantiles with the rainfall quantiles by matching return periods and matching durations, i.e. setting $T_q = T_P = T$ and $d_q = d_P = d$. This comparison does not imply a relationship of rainfall and streamflow of individual events. Instead it examines the similarities of the two distributions irrespective of the time extreme rainfall and floods occur. The equivalence of T_q and T_P seems an obvious choice for comparing the two distributions, because it is a traditional assumption in design methods (e.g. design storm method). Again, this assumption does not imply that T_q and T_P of a single event are identical (which is often not the case, see for example Alfieri et al., 2008; Rahman et al., 2002, Viglione et al., 2009). Instead, it provides a

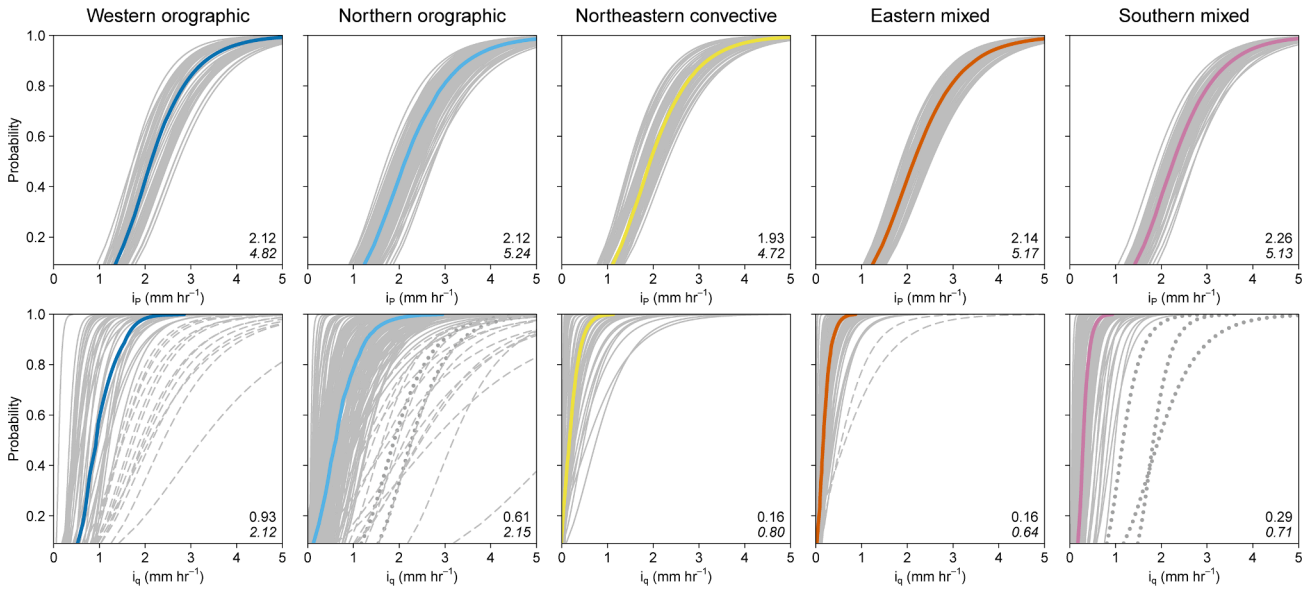

Fig. 6. Cumulative distribution functions of rainfall i_P (upper row) and specific streamflow i_q (bottom row) extremes with a duration of 24hrs in the five rainfall regions. Colored lines represent the median CDFs in each region, numbers in the plot area refer to the 5% and 99% quantiles (italic) of the median. Dashed and dotted grey lines represent catchments impacted by Karst springs and glaciers, respectively (see Fig. 1b).

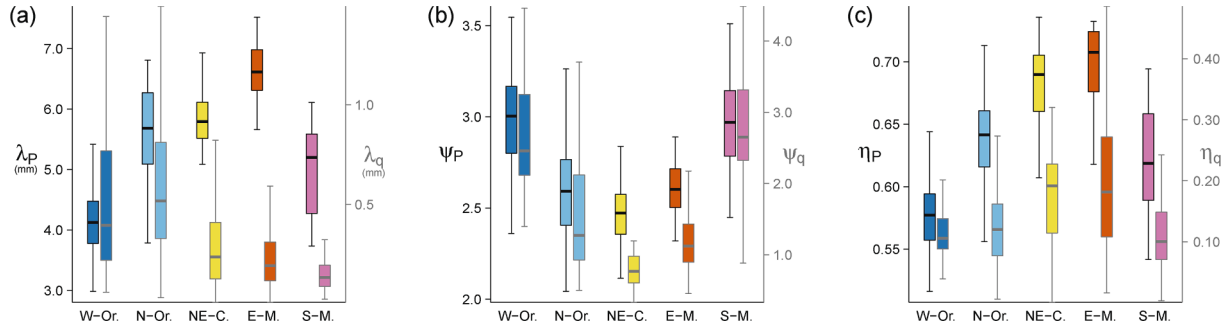

Fig. 7. Distribution of rainfall and streamflow model parameters in five rainfall regions in Austria (Fig. 1b). Left boxplot in each region refers to the rainfall model parameters, right boxplot to the streamflow model parameters. (a) Scale parameters λ_P and λ_q of the rainfall and streamflow model, respectively. (b) location parameters ψ_P and ψ_q. (c) scaling parameters η_P and η_q.

common reference point of the distributions. The assumption of setting $d_q = d_P$ is less obvious, given that one is usually interested in $d_q = 0$ while accounting for various d_P. We have chosen here to set d_q equal to d_P, to allow for a more generalized comparison that goes beyond the flood peak distribution. However, careful consideration of the implications of this assumption is necessary (also see discussion).

Making the above assumption and by combining Equations (2) and (3), we can now plot, for each catchment, the rainfall-flood probability relationship $i_q(i_P, T, d)$ (Fig. 2), where constant duration d and constant return period T are represented by dashed black and dotted red lines, respectively.

In order to characterize the behavior of the $i_q(i_P, T, d)$ relationship, we evaluated the elasticity of streamflow to changes in rainfall as a function of T and d. We first expressed the relationship in terms of d const., which is defined as:

$$i_q(i_P) = d^{-\eta_q}\lambda_q\left(\frac{d^{\eta_P}\cdot i_P}{\lambda_P} - \psi_P + \psi_q\right) \quad (7)$$

$$\text{with } \lambda_P > 0; \lambda_q > 0; d \geq 1hr; 0 < \eta_P < 1; 0 < \eta_q < 1$$

If d = const., Equation (7) has a constant slope $\frac{\lambda_q d^{\eta_P}}{\lambda_P d^{\eta_q}}$ (as reflected by the dashed black lines in Fig. 2). From Equation (7), the elasticity ε_1 of streamflow relative to changes of rainfall assuming d = const. is obtained as:

$$\varepsilon_1 = \frac{\partial i_q(i_P)}{\partial i_P}\cdot\frac{i_P}{i_q(i_P)} = \frac{d^{\eta_P} i_P}{\lambda_P\left(\frac{d^{\eta_P} i_P}{\lambda_P} - \psi_P + \psi_q\right)} \quad (8)$$

$$\text{with } \lambda_P > 0; d \geq 1hr; 0 < \eta_P < 1; \lim_{i_P\to\infty}\varepsilon_1 = 1$$

Interestingly, ε_1 depends neither on the streamflow scale parameter λ_q nor on the streamflow scaling parameters η_q. By inserting i_P into Equation (8), ε_1 can also be expressed in terms of T as

$$\varepsilon_1 = \frac{\psi_P + u}{\psi_q + u}, \text{ with the Gumbel reduced variate} \quad (9)$$

$$u = -\ln\left[-\ln\left(1 - \frac{1}{T}\right)\right]; \lim_{T\to\infty}\varepsilon_1 = 1$$

which indicates that ε_1 is only a function of the return period and the location parameters. For CV_P=CV_q, $\varepsilon_1 = 1$. On the other hand, expressing the $i_q(i_P, T, d)$ relationship in terms of T = const. (red dotted lines in Fig. 2) gives:

$$i_q(i_P) = \lambda_q\left(\frac{i_P}{\lambda_P(\psi_P + u)}\right)^{\frac{\eta_q}{\eta_P}}(\psi_q + u) \quad (10)$$

$$\text{with } \lambda_P > 0; \lambda_q > 0; T \geq 1; 0 < \eta_P < 1; 0 < \eta_q < 1$$

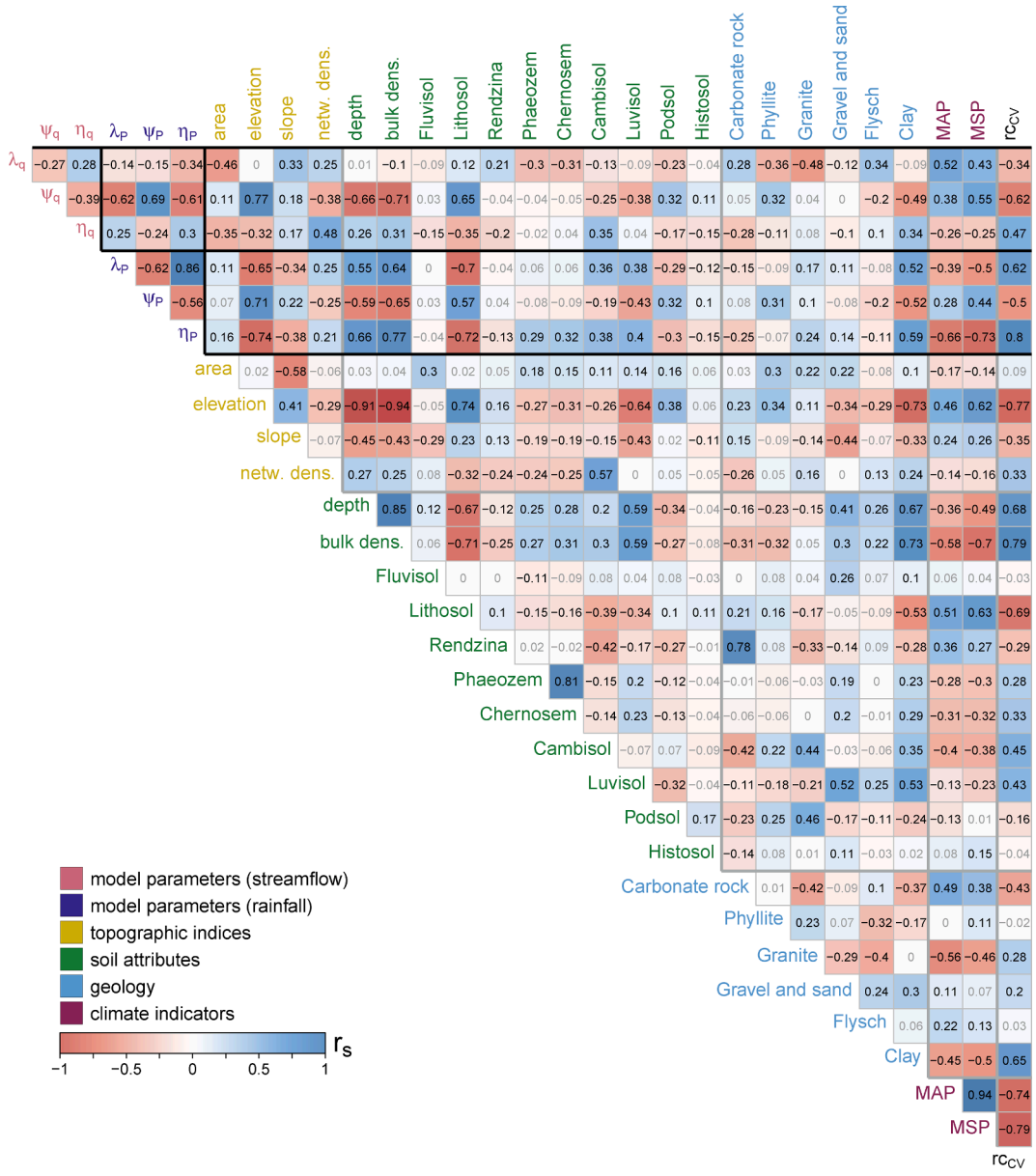

Fig. 8. Spearman rank correlations r_s between streamflow model parameters, rainfall model parameters, topographic indices, soil attributes, geology and climate indicators in 428 catchments (Table 1). The streamflow model parameters are λ_q (scale parameter representing streamflow variability), ψ_q (location parameter representing the magnitude, ceteris paribus) and η_q (scaling parameter representing flashiness of catchment response). The rainfall parameters are λ_P (scale parameter representing rainfall variability), ψ_P (location parameter representing the magnitude, ceteris paribus) and η_P (scaling parameter as an indicator of convective activity). For rc_{CV}, only 342 of the 428 catchments could be analyzed. Correlation coefficients significant at the 5% level are in black font.

from which the elasticity ε_2 for T = const. is obtained as:

$$\varepsilon_2 = \frac{\partial i_q(i_P)}{\partial i_P} \cdot \frac{i_P}{i_q(i_P)} = \frac{\eta_q}{\eta_P} \tag{11}$$

To give a more intuitive illustration of the IDF-QDF relationship, we performed simulations convoluting an observed rainfall time series (43 years) with a linear reservoir, and analyzing the resulting hydrographs according to Equation (3). Fig. 3a shows the mapping of IDF and QDF curves for d = 1hr and different return periods T implicit in the magnitudes of i_q and i_P. For the limiting case of a response time of 0 (i.e. storage coefficient of the linear reservoir k = 0) and a runoff coefficient r_c = 1, streamflow is equal to rainfall and the relationship plots on the 1:1 line. As k increases, the streamflow event peaks decrease and so does i_q. Fig. 3b shows the relationship for $T_q = T_P$ = 2yrs and different durations d implicit in the magnitudes of i_q and i_P. Again streamflow decreases with increasing k, particularly for short durations. For long durations, as demonstrated through experiments assuming block rainfall and varying storm durations d_s (Blöschl & Sivapalan, 1997), the decrease is less pronounced because in a linear system the peak is approximately proportional to d_s/k, which is similar to our approach using different aggregation intervals, i.e. d/k.

The simulations also allow an illustration of the behavior of the elasticities ε_1 and ε_2. For a storage coefficient k = 0 and a runoff coefficient rc = 1, both ε_1 and ε_2 are unity, due to the 1:1 mapping of precipitation to streamflow, meaning a 1% change in rainfall relates to a 1% change in streamflow (Fig. 3c). With increasing k, the elasticity ε_1 decreases to about 0.85. This is because, with higher k, rainfall in the time steps adjoining the annual maxima becomes increasingly more relevant in determining the maximum annual streamflow due to the convolution of the linear reservoir. While for small k the annual maxima of the rainfall and streamflow mostly occur on the same day, this synchronicity

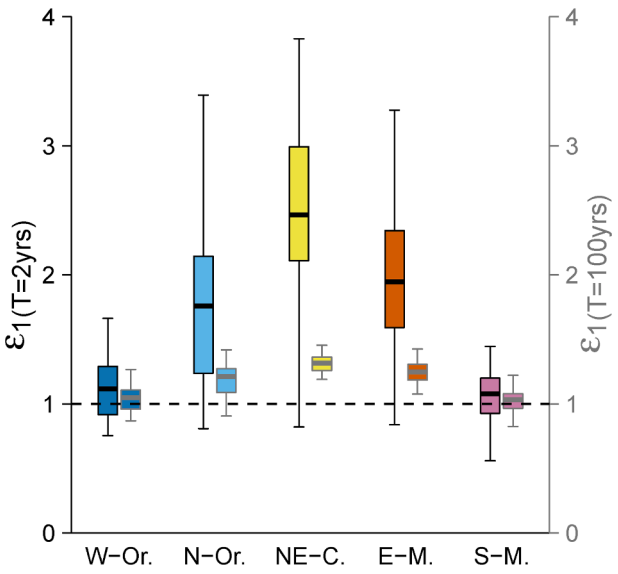

Fig. 9. Elasticity ε_1 of extreme streamflow to changes in extreme rainfall assuming d = const. in five rainfall regions (Fig. 1b), plotted for d = 1hr and the return periods T = 2yrs (left boxplot in each region) and d = 1hr and T = 100yrs (right boxplot in each region). Elasticity is the change in percentage of i_q when i_P is increased by 1%. Boxes represent the 25th and 75th percentiles, lines within the median.

of date of occurrence is lost with increasing k. In the case of ε_2, the decrease of the elasticity with k is more pronounced (from 1 to about 0.1), which relates to the above described dependence of the peak reduction on d/k.

In order to test the sensitivity of the elasticities to the presence of randomness in the runoff coefficient, we assumed the runoff coefficient for each event (defined as rainfall wet spell) to vary randomly between 0 and 1 according to a beta distribution with a mean of 0.29 ($\alpha = 2, \beta = 5$) instead of using rc = 1 (Fig. 3c and Fig. 3d). These values of α and β are representative of medium rainfall regions in Austria (Merz et al., 2006). Random rc increase the elasticity ε_1, which is related to the possibility of combinations of large rainfall with large runoff coefficients, which steepens the flood frequency curve and thus increases ε_1 (Viglione et al., 2009). More skewed beta distributions led to an even larger increase of the elasticity ε_1 (not shown here). On the other hand, the runoff coefficient has little influence on ε_2, as it does not modulate the interplay of k and d.

For our analyses, instead of using the nearest rain gauge to each catchment, we interpolated the parameters of the rainfall model (Equation (2)) to the catchment centroids, to be able to make use of all rain gauges (as in some cases the same rain gauge would be assigned to multiple catchments). We used kriging with external drift (elevation was used as auxiliary variable as it outperformed ordinary kriging) by means of the statistics package "gstat" version 2.0.2 of R version 4.0.3 (Pebesma & Wesseling, 1998). We compared the IDF curves from interpolated rainfall parameters with those of the rain gauge nearest to the catchment centroid and they were similar.

3.3. Correlation analysis

In order to interpret the elasticities in the context of comparative hydrology, we correlated the rainfall model parameters ($\lambda_P, \psi_P, \eta_P$) and streamflow model parameters ($\lambda_q, \psi_q, \eta_q$) with catchment attributes, climate indicators and event runoff coefficients (Table 1). Topographic indices were taken from a digital elevation model of Austria (Rieger, 1999). The river network density was estimated from a digital river network map at a scale of 1:50000 (Fürst, 2003). Soil depth and bulk density were obtained from the ISRIC (International Soil Reference Information Centre) World Soil Information database "SoilGrids" (Hengl et al., 2017). Soil groups were obtained from a digital soil map for Austria (Österreichische Bodenkundliche Gesellschaft, 2001). Geology of each catchment was taken from a digital geological map of Austria (Weber et al., 2019). Long-term mean annual (MAP) and mean seasonal summer rainfall (MSP) based on more than 1,000 daily rainfall gauges were taken from Parajka et al. (2005). Event runoff coefficients as analyzed by Merz et. al. (2006) were available in 342 of the 428 catchments for the summer season for an average of 131 event runoff coefficients per catchment.

3.4. Significance tests

To support the analysis of regional differences of the model parameters and the elasticities, we applied the non-parametric Kruskal–Wallis test to examine whether parameters/elasticities of different regions originate from the same distribution (Kruskal & Wallis, 1952). The test does not assume normally distributed residuals. Additionally, we applied Dunn's Multiple Comparison test (Dunn, 1964) with a Bonferroni correction of the experiment-wise error rate (e.g. Armstrong, 2014) to identify which pairs of the regions are significantly different.

4. Results

4.1. Rainfall model parameters and rainfall mechanism

We first investigated the estimated parameters of the rainfall model (Equation (2)). There is a negative dependency between the scale parameter λ_P and the location parameter ψ_P (Fig. 4a) (Spearman correlation $r_s = -0.62$, p less than 0.05). This dependency seems to be related to regional differences in the rainfall processes. Annual rainfall extremes in the West (dark blue points in Fig. 4) tend to be large with little variability (high ψ_P, small λ_P). In the East (yellow and red points in Fig. 4), annual rainfall extremes tend to be small (small ψ_P) but high rainfall extremes are still possible (high λ_P). There is a positive dependency between λ_P and the scaling parameter η_P ($r_s = 0.86, p < 0.05$) (Fig. 4b) with the western regions exhibiting low η_P and λ_P and the eastern regions exhibiting high η_P and λ_P. This pattern is aligned with the dominance of orographic rainfall in the West and that of convective rainfall in the East. A negative dependency between ψ_P and η_P ($r_s = -0.56, p < 0.05$) exists, i.e. high rainfall amounts (high ψ_P) are related to rainstorms that are less peaky (small η_P) (Fig. 4c).

4.2. Comparison of rainfall and streamflow

Cumulative distribution functions (CDFs) of the rainfall and streamflow extremes stratified by the five rainfall regions are given in Fig. 5 and Fig. 6. At a 1hr duration (Fig. 5, top), the CDFs of rainfall tend to be flatter in the orographic regions (e.g. Western orographic) than in the regions more strongly influenced by convective mechanisms (e.g. Eastern mixed). The streamflow CDFs in the Northeastern, Eastern and Southern regions represent smaller values than in the West and North, which is much more a reflection of runoff generation and routing than of rainfall given the rather similar rainfall CDFs. Moreover, streamflow CDFs are considerably steeper in the East compared to the West: for example, the median streamflow at the 99% percentile is 4.9 times higher than at the 5% percentile in the Northeastern convective zone, while it is only 2.3 times higher in the Western orographic region. The shapes of the streamflow CDFs within each region are more diverse than those of rainfall (Fig. 5, bottom row), again reflecting runoff generation and routing processes. The catchments indicated by dashed and dotted lines are impacted by Karst springs and glaciers, respectively, which further increase the within-region variability. At a duration of 24hrs, intensities of rainfall and streamflow are lower, as expected. However, the steepness (i.e. the CV) of the 24hr and 1hr durations are the same, as

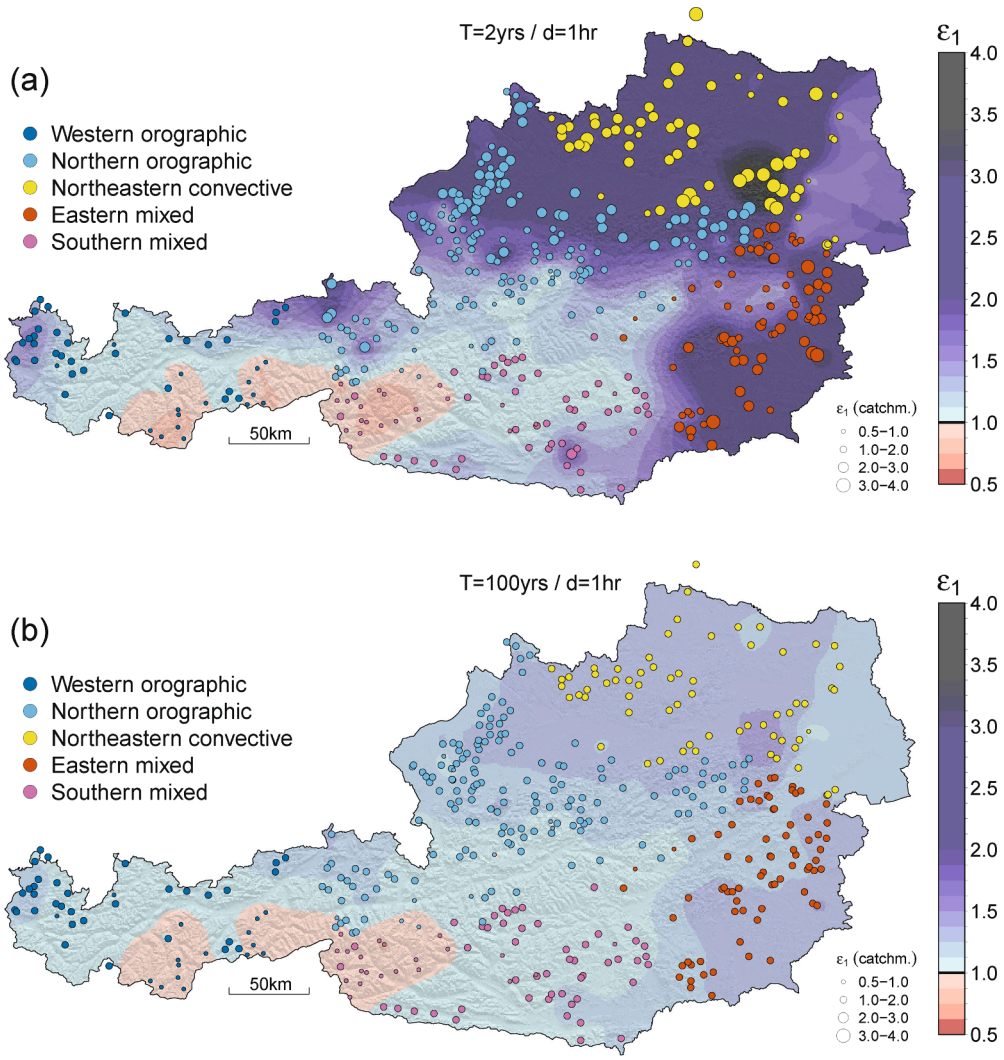

Fig. 10. Elasticity ε_1 of extreme streamflow i_q to changes in extreme rainfall i_P assuming duration d = const. = 1hr in Austria. Elasticity is the change in percentage of i_q when i_P is changed by 1% and is shown as points for each gauged catchment where the sizes represent the values of the elasticities and the colors the rainfall regions (Fig. 1b). Elasticities interpolated from these catchment values (ordinary kriging) are shown as background pattern. (a) ε_1 d = 1hr at T = 2yrs, (b) ε_1 d = 1hr at T = 100yrs.

the scaling models (Equations (2) and (3)) apply the same Gumbel distribution scaled over different durations. The majority of karstic and glaciated catchments exhibit higher streamflow intensities compared to the rainfall. These may be related to factors other than rainfall such as glacier melt and differences between orographic and hydrologic catchment area.

The rainfall and streamflow model parameters reflecting the rainfall and flood intensities (shown in Fig. 5 and Fig. 6) are given in Fig. 7 (corresponding maps in Fig. A3). The "Eastern mixed" region exhibits the highest values of the scale parameter λ_P, reflecting the high variability of rainfall extremes, while the variability of streamflow extremes (λ_q) is highest in the Northern orographic region (Fig. 7a, also see Fig. A3a, b). Hence, the variability of streamflow extremes is spatially not aligned with that of the rainfall extremes.

The location parameters ψ_P and ψ_q (Fig. 7b) have a similar spatial distribution (r_s = 0.69). Both are smallest in the Northeastern convective region and largest in the Western orographic and the Southern mixed regions. Both parameters are highest in the high elevation zones of Austria (Fig. A3c, d). This result can be interpreted as the influence of orographic rainfall and perhaps also higher runoff coefficients (Merz & Blöschl, 2009b). Also, as ψ_P and ψ_q define the CV of the extremes (see Equation (6)), one can conclude that the CV of rainfall is higher in the lowlands influenced by convective mechanisms compared to the alpine orographic regions. The CV of streamflow is likewise higher in the dry lowlands and decreases with increasing elevation (and thus increasing annual rainfall), possibly due to the smaller variability of runoff coefficients (Merz & Blöschl, 2009b). The lowest CV of streamflow occurs in the glaciated areas as the values of ψ_q are the highest (also see Fig. 1a). Thus, as opposed to the scale parameters (see above), the CVs of rainfall and floods are spatially aligned.

The scaling parameters of the streamflow η_q are generally lower than the ones of the rainfall (η_P) reflecting the dampening effects of catchment processes (Fig. 7c). Moreover, η_P and η_q are spatially aligned with the largest values in the Northeastern convective and Eastern mixed regions. This behavior reflects the higher convective activity and flashier flood response (also see Fig. A3e, f). There are striking similarities between the spatial distribution of η_q and the concentration times of catchments as analyzed by Gaal et al. (2012) from flood events (Gaal et al. (2012), Fig. 4), which is not surprising as η_q reflects the catchment response time.

Dunn's multiple comparison test (Table A1) reveals that parameters are often significantly different at the 5% level between the Alpine regions and the lowlands (e.g. between the Northeastern convective region and the Southern mixed region), whereas within these two major zones, significant differences of fewer parameters are identified (e.g. between the Western orographic regions and the Southern mixed region).

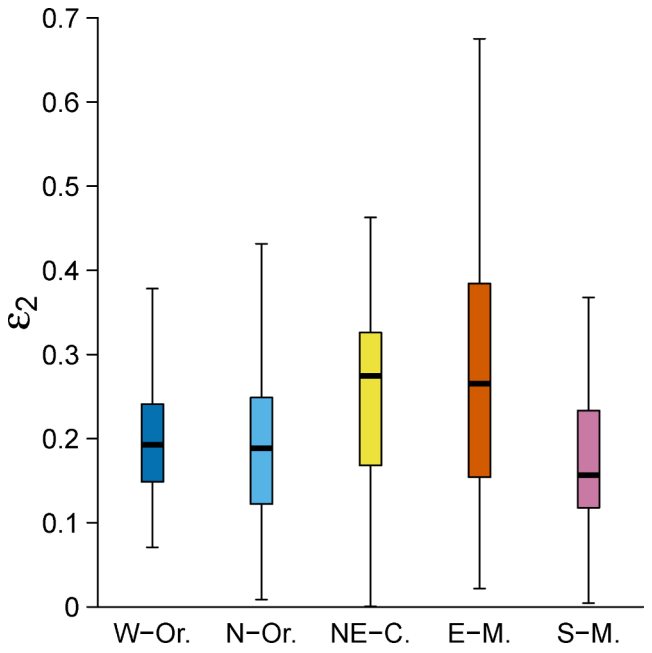

Fig. 11. Elasticity ε_2 assuming T = const. of streamflow to rainfall extremes of all catchments in the five rainfall regions in Austria (Fig. 1b). Elasticity is the change in percentage of i_q when i_P is increased by 1%. Boxes represent the 25th and 75th percentiles, lines within the median.

4.3. Spatial correlation of model parameters

The statistical properties of the streamflow extremes can only be partly explained by the properties of extreme rainfall. Other potential controls include catchment topography, soil properties, geology and long-term climate. All of these controls are assessed by the correlation analysis of Fig. 8. All correlations discussed below are significant at the 5% level.

The correlation between the scale parameter of streamflow λ_q and that of rainfall λ_P is low, as would be expected from Fig. 7a, but higher correlations of λ_q exist with catchment area ($r_s = -0.46$) and mean topographic slope ($r_s = 0.33$), suggesting that streamflow extremes are more variable in small and in steep than in large and flat catchments. λ_q is negatively correlated with soils of high water holding capacity such as Phaeozem and Chernosem (IUSS Working Group WRB, 2015) ($r_s = -0.30$ and $r_s = -0.31$), suggesting that pervious soils reduce streamflow variability. Reduced variability can also be detected for Phylitte geology ($r_s = -0.36$), which is a deeply weathered metamorphic rock with deep flow paths and slow flood response (Gaal et al., 2012). Furthermore, a positive correlation exists between λ_P and the CV of the event runoff coefficients rc_{CV} ($r_s = 0.62$) as well as λ_P and the skewness of the event runoff coefficients rc_{CS} ($r_s = 0.51$), suggesting that the latter are more variable and skewed in regions of increased rainfall variability.

The location parameter of streamflow ψ_q is positively correlated with the location parameter of rainfall extremes ψ_P ($r_s = 0.69$, in line with Fig. 7b) , mean annual (MAP) and summer rainfall (MSP) ($r_s = 0.38$ and $r_s = 0.55$), which can be interpreted through rainfall mechanisms: MAP and MSP increase with mean catchment elevation due to orographic effects (e.g. $r_s = 0.62$ between MSP and elevation), which is consistent with the positive correlation between elevation and ψ_P ($r_s = 0.71$). ψ_q and ψ_P are negatively correlated with rc_{CV} ($r_s = -0.62$ and $r_s = -0.5$) and with rc_{CS} ($r_s = -0.5$ and $r_s = -0.41$), suggesting that event runoff coefficients tend to be less variable and less skewed in regions of high rainfall amounts.

The scaling parameter η_q is positively correlated with that of precipitation η_P ($r_s = 0.30$) pointing towards a relationship between the convective activity of rainfall and the flashiness of catchments. However, there are higher absolute correlations between η_q and catchment area ($r_s = -0.35$) and the stream network density ($r_s = 0.48$), which suggests that the flashiness of streamflow hydrographs decreases with catchment area and increases with stream network density, as would be expected.

4.4. Elasticities

The elasticity ε_1 of streamflow relative to changes of the rainfall assuming d = const. (Equation (8)) is characterized by a distinct spatial pattern (Fig. 9 and Fig. 10). The elasticities ε_1 are shown in Fig. 9 as boxplots and in Fig. 10 as maps. The sizes of the points in Fig. 10 represent the values of ε_1 for each gauged catchment (at the catchment centroids), the background pattern is generated by interpolation from these catchment values (ordinary kriging) and is intended to better highlight the regional patterns. For T = 2yrs, the rainfall-streamflow relationships are highly elastic (i.e. $\varepsilon_1 \gg 1$) in the lowlands in the North, Northeast and Southeast (e.g. Northeastern convective rainfall region) compared to the high Alpine regions (e.g. Western orographic

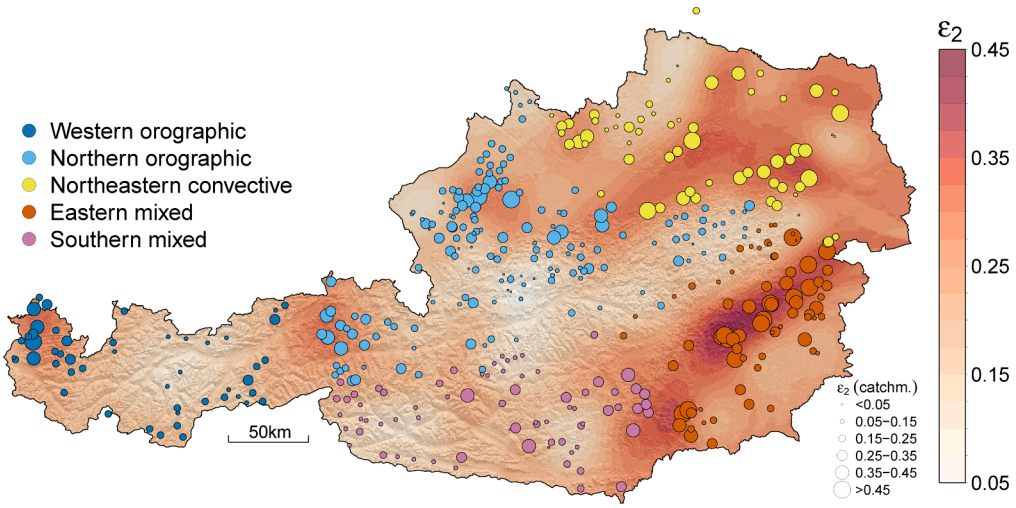

Fig. 12. Spatial patterns of the elasticity ε_2 of all catchments assuming T = const. for the five rainfall regions in Austria (Fig. 1b). Elasticity is the change in percentage of i_q when i_P is increased by 1% and is shown as points for each gauged catchment where the sizes represent the values of the elasticities and the colors the rainfall regions (Fig. 1b). Elasticities interpolated from these catchment values (ordinary kriging) are shown as background pattern.

region) where the elasticity is closer to unity i.e. $\varepsilon_1 \sim 1$ (left boxplots of Fig. 9 and Fig. 10a). In the glaciated regions of the highest summits of Austria (regions in red colors in Fig. 10, also see glaciated areas in Fig. 1a) the relationships are inelastic ($\varepsilon_1 < 1$). For a return period of T = 100yrs (right boxplots in Fig. 9 and Fig. 10b), the spatial pattern remains similar, but the elasticities tend towards unity.

Although our approach of analyzing the rainfall-flood relationship refers to a comparison of distribution functions rather than individual events, we additionally analyzed the synchronicity of the dates of annual rainfall and streamflow extremes, in order to explore whether the event producing the largest annual streamflow are often the same as those producing the largest rainfall. To this end, stream gauges were compared to the nearest rain gauges, with at least ten years of recording overlap. Fig. A4 shows the percentage of annual rainfall and streamflow maxima that occurred within 24hrs of each other for the duration of 1hr (left boxplots) and 24hrs (right boxplots), stratified by rainfall regions. The synchronicity of both durations is highest in the lowlands of the North and East, which are regions of flashy catchment response represented by large η_q (Fig. A3f). In these regions, also elasticities ε_1 (Fig. 9) are highest. This is in line with our simulation experiments (Fig. 3c), which indicated small storage coefficients k to cause high elasticities ε_1. On the other hand, synchronicities are smallest in the Alpine regions (e.g. Western orographic region) where values of η_q are low.

The elasticity ε_2 of streamflow relative to rainfall changes assuming T = const. (Equation (11)) is highest in the dry lowlands in the Northeast and East (Northeastern convective and Eastern mixed rainfall region) (Fig. 11 and Fig. 12). As in the case of Fig. 10, the sizes of the points in Fig. 12 represent the values of ε_2 for each gauged catchment (at the catchment centroids), while the background pattern is generated by interpolation from these catchment values (ordinary kriging). In these regions catchment concentration times tend to be short as indicated by high η_q (Fig. 7c), and storm durations tend to be short indicated by high η_P (as high values η_P indicate fast decrease of rainfall intensity with duration), also indicated by the short average wet spell duration in Fig. A2b). Generally, the closer ε_2 is to unity, the more similar is the duration of flood triggering rainstorms and the concentration time of the catchment (Equation (11)). On the other hand, the elasticities ε_2 in the Alpine regions (e.g. Northern orographic region) are lower.

The pronounced similarities of the spatial patterns of ε_1 (Fig. 10) and the location parameter of the streamflow ψ_q (Fig. A3d), as well as the spatial patterns of ε_2 (Fig. 12) and the scaling parameter of the streamflow η_q (Fig. A3f) suggest that catchment processes dominate the runoff transformation, since ε_1 is defined by the location parameters (Equation (9)) and ε_2 by the scaling parameters (Equation (11)). The dominance of catchment processes is also visible in the cumulative distribution functions of rainfall and streamflow (Fig. 5 and Fig. 6), with more pronounced differences between the CDFs of the streamflow of different regions compared to the rainfall. Moreover, the elasticity ε_1 (T = 2yrs) is positively correlated with the CV of the event runoff coefficients rc_{CV} ($r_s = 0.59$) and the skewness of the runoff coefficients rc_{CS} ($r_s = 0.49$), indicating that ε_1 is increased in regions of more variable and skewed runoff coefficients. Dunn's multiple comparison test (Table A1) reveals that there are no significant differences between ε_1 in the Alpine Western orographic and Southern mixed regions. The situation is similar for ε_2, where no statistically significant differences can be detected between the Alpine Western orographic, Northern orographic and Southern mixed regions, and between the Northeastern convective and the Eastern mixed regions. As with the model parameters, it appears that the regional differences of the elasticities can be broadly generalized into differences between the precipitation-rich Alps and the dry lowlands.

5. Discussion

Our analyses based on the concept of comparative hydrology unravel the most important factors, including dominating rainfall and catchment characteristics that control the differences between the distributions of rainfall and streamflow extremes.

The moments and parameters of the rainfall distribution are aligned with the regional rainfall mechanisms. In the high elevation catchments where orographic rainfall dominates, the location parameter ψ_P tends to be high and the scale parameter λ_P tends to be small, i.e. the rainfall extremes tend to be large with little temporal variability (see Fig. A3a and A3c). The opposite applies to catchments in the lowlands where convective rainfall extremes are more frequent. The relationship between rainfall magnitude and variability is reflected by a high negative correlation between ψ_P and λ_P (Fig. 4a and Fig. 8, $r_S = -0.62$). The regional rainfall mechanisms also manifest themselves in the spatial distribution of the scaling parameter η_P, which tends to be higher in the convective lowlands than in the mountainous regions with dominant orographic rainfall (Fig. A3e). A higher parameter η_P implies that the intensity decreases more strongly with duration which can be expected for the short rainstorms that occur frequently in the lowlands.

As in the case of rainfall, the location parameter of streamflow ψ_q is higher in the mountain catchments than in the lowlands (see Fig. A3d), reflected by a strong positive correlation of ψ_q with catchment elevation (Fig. 8, $r_S = 0.77$) and mean summer rainfall (Fig. 8, $r_S = 0.55$). This means, the magnitude of floods tends to be higher in the orographic rainfall regions, not only due the higher extreme rainfall magnitudes but also due to high annual rainfall amounts, possibly leading to high soil moisture levels, persistently high runoff coefficients and to a propensity towards saturation excess overflow. The variability of streamflow represented by the scale parameter λ_q, however, is controlled by catchment topography, soil type and the geology (e.g. correlations with slope $r_S = 0.33$, Rendzina soils $r_S = 0.21$ or Carbonate rock geology $r_S = 0.28$, Fig. 8) and is thus highest along the Alpine ridge (Fig. A3b), while the variability of the rainfall represented by λ_P is mainly controlled by elevation (see negative correlation between λ_P and elevation in Fig. 8) and is highest in the lowlands (Fig. A3a). Some of the highest values of λ_q relate to karstic catchments along the Alpine divide (see Fig. 1a catchments with crosses, Fig. A3b and positive correlation between λ_q and Carbonate rock in Fig. 8). In karstic catchments, during periods of average rainfall events, most of the rainfall may be stored in the fractured carbonic rocks, while more extreme rainfall events can saturate the epikarst zone inducing large streamflow extremes (Li et al., 2017) and thus more variable floods. Such step changes in streamflow extremes may also occur in other geological formations (Rogger et al., 2012). The scaling parameter η_q (Fig. A3f), on the other hand, is highest in the lowlands, showing a similarity with the spatial distribution of the rainfall scaling parameter η_P, which is also lowest in the lowlands.

For the comparison of rainfall and flood distributions, one can conclude, not surprisingly, that higher rainfall extremes tend to lead to higher floods, as the positive correlation between the location parameters ψ_P and ψ_q indicates (Fig. 8, $r_S = 0.69$). This relationship is more distinct in regions dominated by orographic rainfall, where runoff coefficients are persistently high (Merz & Blöschl, 2003), such as in the Northern orographic region ($r_S = 0.70$). The relationship is not existent in the Northeastern convective region, where runoff coefficients tend to be lower and more random (Merz & Blöschl, 2003) ($r_S = 0.01$). In this context, the relationship between ψ_P and elevation is also more distinct for the Alpine orographic regions (e.g. correlation between ψ_P and elevation $r_s = 0.81$ in the Northern orographic region) than in the convective lowlands (e.g. $r_s = 0.35$ in the Northeastern convective region), which is in line with Barbero et al. (2019) who found stronger positive correlation between expected values of daily rainfall compared to hourly rainfall, as the former integrate large-scale dynamics and orographic effects (Barbero et al., 2019).

Since the CV is a direct function of the location parameter, similar correlations apply between CV_q and CV_P. In other words, a steeper rainfall frequency curve is associated with a steeper flood frequency

curve, which is in line with previous studies (e.g. Merz & Blöschl, 2003; Smith et al., 2011; Villarini & Smith, 2010). The scale parameter of rainfall is not aligned with that of streamflow, reflected by $r_S = -0.14$ between λ_P and λ_q and different spatial patterns (Fig. A3a, A3b and Fig. 8).

The spatial patterns of the scaling parameters η_P and η_q are to some extent aligned (Fig. 8, $r_S = 0.3$) with larger parameters in the North and East and lower in the West. This similarity suggests that the response times of catchments to the storms producing the annual floods tend to be shorter in regions dominated by convective activity (North and Northeast), while the opposite is the case in the West. The similarity is possibly due to an interplay of climatic and catchment processes over time, modulated by the geology (Gaal et al., 2012). For example, the efficient drainage network in the Southeast of Austria leads to short response times and may have evolved from the dominating convective rainfall mechanisms in the region (see for example high frequency of hailstorms in Fig. A1) as intense convective rainstorms increase the overland flow, which in return influences the drainage network (Abrahams & Ponczynski, 1984; Tucker & Bras, 2000).

We quantified the relationship between rainfall and flood probabilities by elasticities. ε_1 represents the percent change of flood discharge for a 1% in extreme rainfall change assuming duration d is constant. Elasticities ε_1 are highest in the dry lowlands in the Northeast and Southeast (Fig. 9 and Fig. 10). For T = 2yrs, they are more than four times higher than the mean of the Alpine catchments. That is, in the dry lowlands, flood frequency curves are considerably steeper than the rainfall frequency curves, which is consistent with the regional analyses (Merz & Blöschl, 2009a, 2009b). Viglione et al. (2009) suggested that in dry regions, steep flood frequency curves can result from the occurrence of extraordinary events with runoff coefficients exceeding by far those of other events in the catchment (Gutknecht et al., 2002; Komma et al., 2007), reflecting a highly skewed distribution of runoff coefficients.

In the mountainous catchments of the study region, where annual rainfall is above 1000 mm yr^{-1}, elasticities ε_1 are closer to unity (Fig. 9 and Fig. 10). In these catchments the high orographic rainfall may frequently lead to soil saturation and thus event runoff coefficients tend to be high (Merz & Blöschl, 2009b), and therefore the steepness of the flood frequency curves is similar to that of the IDF curves. Another possible explanation is the slower catchment response in parts of the high rainfall regions (Gaal et al., 2012), as a result of a more pervious geology, for example in the Southern mixed rainfall zone where the Phylitte geology reduces the response time (Fig. 1c) and thus may reduce elasticity as illustrated in the simulation experiment (Fig. 3). This is because, for slow response times, the highest rainfall extreme of year and a given duration does not necessarily cause the highest flood peak in that year. The lower correspondence of rainfall and flood events is also in line with their lower synchronicity (Fig. A4). The decoupling is even more pronounced in the glaciated catchments (Fig. 10 red areas) where elasticities drop below unity, as a consequence of glacier melt that is more relevant to floods than rainfall extremes.

ε_2 represents the percent change of flood discharge for a 1% change in extreme rainfall assuming the return period T is constant. In the model ε_2 is represented by $\frac{\eta_q}{\eta_P}$ (Equation (11)), i.e. the ratio of the temporal scaling of streamflow and extreme rainfall. Regions of high elasticities ε_2 are regions of fast catchment response as indicated by (Gaal et al., 2012), which is aligned with values of η_q and to some degree η_P (Fig. 11, Fig. 12, and Fig. A3f). Fast catchment response is mainly related to shallow soils, and clay and marl and Flysch geologies with low infiltration (Fig. 1c), as well as an efficient drainage network (Gaal et al., 2012; Holko et al., 2011). In these regions, also relevant storm durations tend to be short due to the dominance of convective rainfall, which in combination with the fast catchment response explains the high elasticities ε_2. Regions of low elasticities ε_2 on the other hand are those with slow catchment response as in the South of the country where the deeply weathered Phylitte geology dominates.

While, to our knowledge, no regional, data-based studies on elasticities of streamflow extremes exist, our results are in line with previous studies on elasticities of annual streamflow that show largest elasticities in dry climates (e.g. Chiew, 2006; Sankarasubramanian et al., 2001; Tang et al., 2019; Yang & Yang, 2011).

Elasticities ε_1 tend towards unit elasticity with increasing return period, as can be seen from Equation (9), Fig. 9 and Fig. 10. This behavior is a consequence of the model formulation and fully consistent with hydrological reasoning. For both, infiltration excess and saturation excess mechanisms, runoff tends to become more similar to rainfall as the rainfall intensity increases, and if soil saturation is reached, any additional rainfall transforms into surface runoff. This behavior implies that the gradients of the tails of the flood and rainfall distribution become similar (i.e. $\varepsilon_1 = 1$), which is the rationale behind the gradex method (Guillot, 1993; Merz & Blöschl, 2008; Naghettini et al., 1996). Our results suggest that this assumption is fully consistent with the combined intensity-duration-frequency analysis adopted here and found suitable for the Austrian data. Given the similarity in runoff generation mechanism in terms of increasing runoff contributions with increasing return period (McDonnell, 2013), it is possible that the tendency towards unit elasticity with increasing return period may hold in many regions throughout the world. However, it may be of interest to test the elasticity behavior using more complex models, both similar combined models but with a larger number of parameters, and joint distribution models such as Copulae (e.g. Balistrocchi & Bacchi, 2011; Klein et al., 2010), which allow for a more flexible description of the intensity-duration-frequency analysis.

In our analysis of elasticities we assumed that the return periods of rainfall and floods are the same. This assumption seems natural given that it provides a common reference point for comparing distributions. We also assumed that the durations of rainfall and floods are the same ($d_q = d_P = d$). However, for the models adopted here (Eq. (2) and (3)), the elasticity ε_1 in fact does not depend on this assumption and is also valid for $d_q \neq d_P$ (see also Equation (9)), as long as $T_q = T_P = T$, $d_q = \text{const.}$ and $d_P = \text{const.}$ It is therefore equally valid for e.g. $d_q = 1\text{hr}$ (approximately representing peak flow), and $d_P > 1\text{hr}$ (representing the various durations of the IDF curve). On the other hand, for ε_2, $d_q = d_P = d$ is a prerequisite, while the assumption $T_q = T_P = T$ is not necessary, but $T_q = \text{const.}$ and $T_P = \text{const.}$ The independences of ε_1 on d and ε_2 on T result from the assumption of self-affinity in the scaling models for rainfall and runoff (equations (2) and (3)), in which the same extreme value distribution is scaled by durations. While these scaling models were found to be suitable for this study region, this may not apply to other regions, where other scaling models, perhaps with more parameters, may be more appropriate.

Our work has various implications. The sensitivity of floods to extreme rainfall as proposed here may be useful when extrapolating to flood frequency distributions beyond observed floods. One possibility would be a Bayesian framework (Costa & Fernandes, 2017; Viglione et al., 2013) which allows incorporating this type of process based information. For such applications it may be worth considering alternative distributions such as the GEV that have more flexibility in the tail behavior. In particular, if the flood distribution is heavy tailed while the associated rainfall distribution is not, the limiting elasticity may be greater than unity. Additionally, there is potential for elasticity analyses in the context of climate impact studies. Analyzing long-term changes of the elasticity of extremes may be useful for detecting long-term variability in rainfall and streamflow time series to assist in hydrological model calibration for changing conditions (Duethmann et al., 2020; Lun

et al., 2020). More generally, the elasticity of extremes may also be used as a benchmark tool for stochastic rainfall-runoff modelling frameworks, for example weather generators coupled with hydrological models (e.g. Bennett et al., 2019; Gao et al., 2020; Müller-Thomy & Sikorska, 2019; Okoli et al., 2019).

6. Conclusion

In this paper, we present a new approach of comparing the rainfall-flood relationship based on quantiles from intensity-duration-frequency models. Instead of comparing the rainfall-flood relationship of individual events (e.g. Viglione et al., 2009), we compare distribution functions of extreme rainfall and streamflow without event-based linkages. For this comparison, we apply the elasticity concept to extreme rainfall and streamflow, which sets the study apart from the traditional application of the elasticity to annual rainfall and streamflow (e.g. Chiew, 2006; Sankarasubramanian et al., 2001; Tang et al., 2019; Yang & Yang, 2011). Our results suggest that the extreme rainfall elasticity to floods behaves similarly to the annual rainfall elasticity to annual streamflow. Elasticities are higher in regions of low annual rainfall (where rainfall events are primarily short and convective) than in regions of high annual rainfall (where rainfall events are longer and more often of orographic nature). These regional differences of elasticities are related to a variety of factors, including the long-term climate, topography, soils and geology. For example, high elasticities in the dry regions are related to more variable and skewed event runoff coefficients, which may be caused by the dominance of infiltration excess mechanisms associated with high rainfall intensities. In future research, it would be interesting to compare the proposed distribution based approach with event based approaches such as those of Viglione et al. (2009), to explore whether the elasticities identified here provide information on how return periods from rainfall and streamflow relate to each other for individual events.

CRediT authorship contribution statement

Korbinian Breinl: Conceptualization, Methodology, Data curation, Software, Writing - original draft, Writing - review & editing. **David Lun:** Conceptualization, Methodology, Writing - review & editing. **Hannes Müller-Thomy:** Conceptualization, Methodology, Writing - review & editing. **Günter Blöschl:** Conceptualization, Methodology, Writing - review & editing.

Declaration of Competing Interest

The authors declare that they have no known competing financial interests or personal relationships that could have appeared to influence the work reported in this paper.

Acknowledgments

Korbinian Breinl received funding from the European Union's Horizon 2020 research and innovation programme under the Marie Sklodowska-Curie grant agreement STARFLOOD No. 793558. David Lun received financial support from the DFG project 'SPATE' (FOR 2416), the FWF project 'SPATE' (I 4776) and the FWF Vienna Doctoral Program on Water Resource Systems (DK W1219-N28). Hannes Müller-Thomy acknowledges the funding from the Research Fellowship (MU 4257/1-1) by DFG e.V., Bonn, Germany. This research also received funding from the Austrian Federal Ministry for Sustainability and Tourism and the Bavarian Environment Agency in the framework of the project WETRAX+. We thank the Central Institute for Meteorology and Geodynamics for providing the rain gauge data and the European Severe Storms Laboratory (ESSL) and Thomas Schreiner for providing historical hailstorm, wind gust and tornado reports of the European Severe Weather Database (ESWD). Rain gauge data are available from the Central Institute for Meteorology and Geodynamics (ZAMG) from https://www.zamg.ac.at/cms/en/climate/climate. River gauge data are available from the Austrian Federal Ministry of Agriculture, Regions and Tourism (BMLRT) from https://www.bmlrt.gv.at/english/water.html. Severe weather data for Austria (ESWD database) can be accessed via https://www.eswd.eu/. The authors acknowledge TU Wien Bibliothek for financial support through its Open Access Funding Programme. Comments by the editor and two anonymous referees that helped to improve an early version of this paper are highly appreciated.

Appendix A

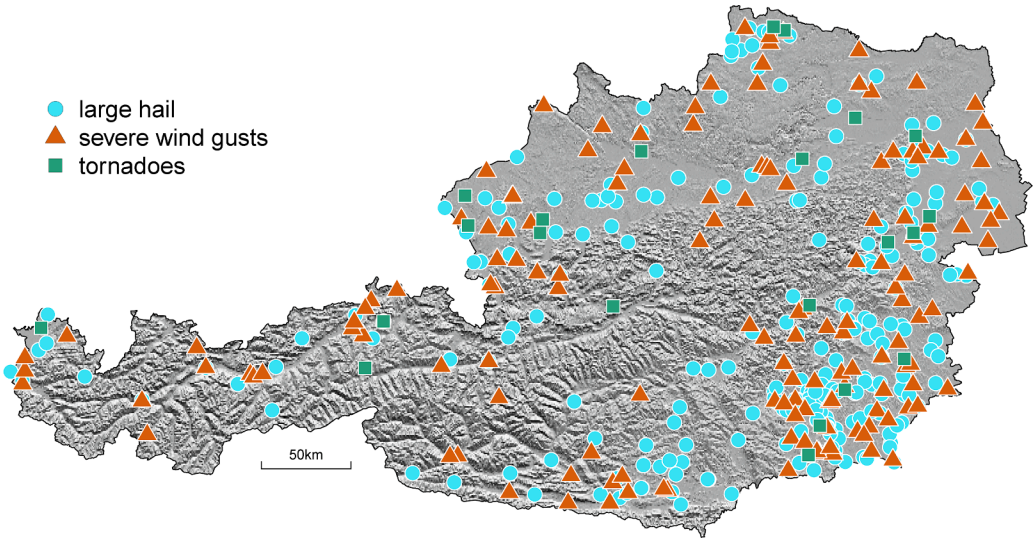

Fig. A1. Locations of large hail events, severe wind gusts and tornadoes in Austria, as reported to the European Severe Weather Database (ESWD) (Dotzek et al., 2009), for the period 1900–2020. In case of multiple locations reported for the same hail or tornado track, the first reported location is shown.

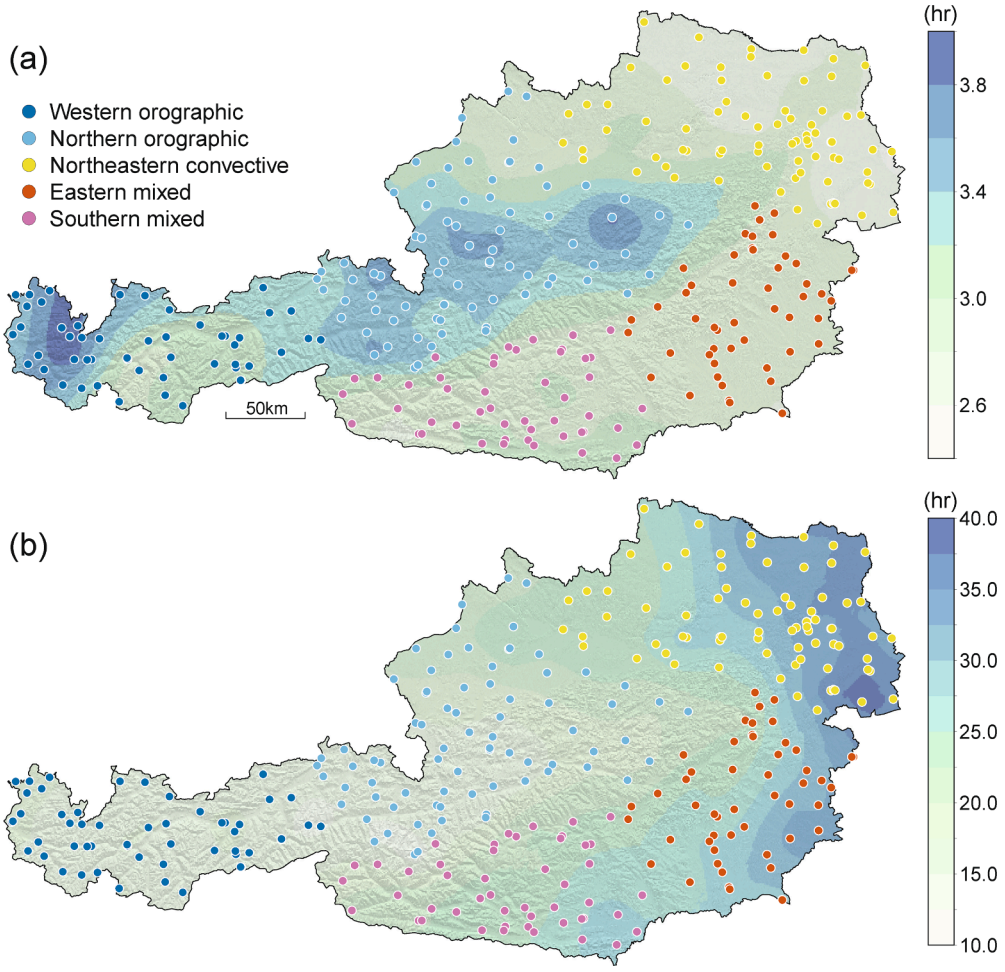

Fig. A2. (Top) Mean duration of rainfall wet spells in summer (June, July, and August) (in hours). (Bottom) Mean duration of rainfall dry spells (in hours). Points represent the rain gauge locations and their colors refer to the five rainfall zones in Austria (Fig. 1b).

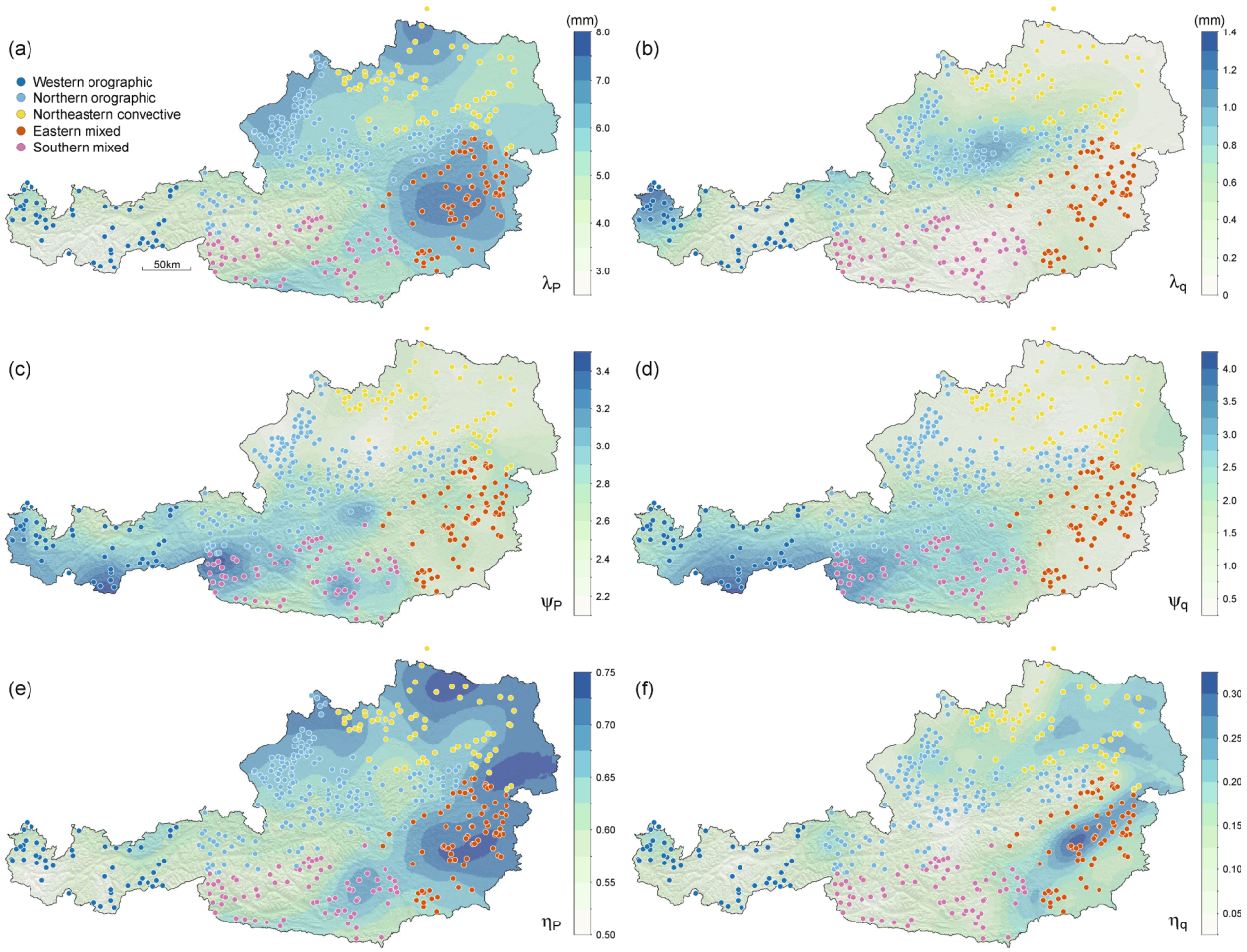

Fig. A3. Spatial patterns of the rainfall model parameters (left panel) and streamflow model parameters (right panel). Colored points for the rainfall parameters represent the rain gauges, colored points for the streamflow parameters represent the centroids of gauged catchments. Coloring of the points represents the five rainfall zones in Austria (Fig. 1b). The rainfall parameters include λ_P (scale parameter representing rainfall variability), ψ_P (location parameter representing the magnitude, ceteris paribus) and η_P (scaling parameter indicating convective activity). The streamflow model parameters include λ_q (scale parameter representing streamflow variability), ψ_q (location parameter representing the magnitude, ceteris paribus) and η_q (scaling parameter representing catchment response).

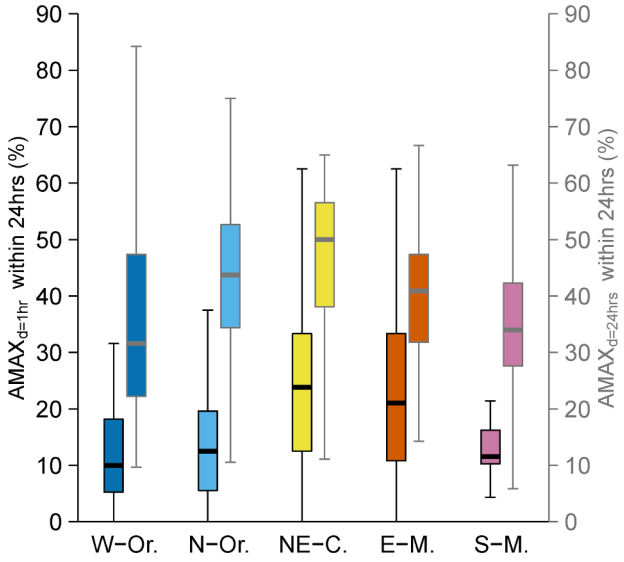

Fig. A4. Synchronicity of rainfall extremes and streamflow expressed as the percentage of annual maxima (AMAX) of rainfall and streamflow recorded within 24hrs for annual maxima of a duration d = 1hr (left boxplot in each region) and a duration of d = 24hrs (right boxplot in each region). Colors of boxplot represent each of the five rainfall regions in Austria (Fig. 1b). Boxes represent the 25th and 75th percentiles, lines within the median.

Table A1
Adjusted p-values (Bonferroni adjustment) from pairwise multiple-comparison of variables (model parameters and elasticities) using Dunn's test, for all possible pairs of the rainfall regions. For each variable, a Kruskal–Wallis test as preliminary analysis was rejected. Codes refer to the rainfall regions: (1) Western orographic, (2) Northern orographic, (3) Northeastern convective, (4) Eastern mixed, (5) Southern mixed.

Parameter	Pairs of rainfall regions									
	1-2	1-3	1-4	1-5	2-3	2-4	2-5	3-4	3-5	4-5
λ_q	0.1197	0.0003	0.0000	0.0000	0.0000	0.0000	0.0000	0.3704	0.0006	0.0079
ψ_q	0.0000	0.0000	0.0000	0.5590	0.0000	0.0160	0.0000	0.0013	0.0000	0.0000
η_q	0.6402	0.0001	0.0000	0.5328	0.0000	0.0000	0.1745	0.7980	0.0000	0.0000
λ_P	0.0000	0.0000	0.0000	0.0004	0.1593	0.0000	0.0000	0.0000	0.0000	0.0000
ψ_P	0.0000	0.0000	0.0000	0.9243	0.0017	0.8541	0.0000	0.0042	0.0000	0.0000
η_P	0.0000	0.0000	0.0000	0.0000	0.0000	0.0000	0.0172	0.103	0.0000	0.0000
ε_1 $(T = 2yrs)$	0.0000	0.0000	0.0000	0.5146	0.0000	0.0042	0.0000	0.0051	0.0000	0.0000
ε_1 $(T = 100yrs)$	0.0000	0.0000	0.0000	0.4824	0.0000	0.0013	0.0000	0.0141	0.0000	0.0000
ε_2	0.4426	0.0190	0.0000	0.1494	0.0001	0.0000	0.3131	0.8944	0.0000	0.0000

References

Abrahams, A.D., Ponczynski, J.J., 1984. Drainage Density in Relation to Precipitation Intensity in the USA. J. Hydrol. 75 (1–4), 383–388. https://doi.org/10.1016/0022-1694(84)90061-1.

Alfieri, L., Laio, F., Claps, P., 2008. A simulation experiment for optimal design hyetograph selection. Hydrol. Process. 22 (6), 813–820. https://doi.org/10.1002/(ISSN)1099-108510.1002/hyp.v22:610.1002/hyp.6646.

Armstrong, R.A., 2014. When to use the Bonferroni correction. Ophthalmic Physiol. Opt. 34 (5), 502–508. https://doi.org/10.1111/opo.12131.

Arnaud, P., Lavabre, J., 2002. Coupled rainfall model and discharge model for flood frequency estimation. Water Resour. Res. 38 (6), 11-1–11-11. https://doi.org/10.1029/2001WR000474.

Awadallah, A.G., 2015. Regional intensity-duration-frequency curves for Jeddah region, Saudi Arabia, using ordinary and L-moments approaches. J. Flood Risk Manage. 8 (3), 195–207. https://doi.org/10.1111/jfr3.12085.

Balistrocchi, M., Bacchi, B., 2011. Modelling the statistical dependence of rainfall event variables through copula functions. Hydrol. Earth Syst. Sci. 15 (6), 1959–1977. https://doi.org/10.5194/hess-15-1959-2011.

Barbero, R., Fowler, H.J., Blenkinsop, S., Westra, S., Moron, V., Lewis, E., Chan, S., Lenderink, G., Kendon, E., Guerreiro, S., Li, X.-F., Villalobos, R., Ali, H., Mishra, V., 2019. A synthesis of hourly and daily precipitation extremes in different climatic regions. Weather Clim. Extremes 26, 100219. https://doi.org/10.1016/j.wace:2019.100219.

Basso, S., Schirmer, M., Botter, G., 2016. A physically based analytical model of flood frequency curves. Geophys. Res. Lett. 43 (17), 9070–9076. https://doi.org/10.1002/2016gl069915.

Bell, V.A., Moore, R.J., 2000. The sensitivity of catchment runoff models to rainfall data at different spatial scales. Hydrol. Earth Syst. Sci. 4 (4), 653–667. https://doi.org/10.5194/hess-4-653-2000.

Benestad, R.E., Nychka, D., Mearns, L.O., 2012. Spatially and temporally consistent prediction of heavy precipitation from mean values. Nat. Clim. Change 2 (7), 544–547. https://doi.org/10.1038/Nclimate1497.

Bennett, B., Thyer, M., Leonard, M., Lambert, M., Bates, B., 2019. A virtual hydrological framework for evaluation of stochastic rainfall models. Hydrol. Earth Syst. Sci. 23 (11), 4783–4801. https://doi.org/10.5194/hess-23-4783-2019.

Berghuijs, W.R., Woods, R.A., Hutton, C.J., Sivapalan, M., 2016. Dominant flood generating mechanisms across the United States. Geophys. Res. Lett. 43 (9), 4382–4390. https://doi.org/10.1002/2016gl068070.

Blöschl, G., Bierkens, M., Chambel, A., Cudennec, C., Destouni, G., Fiori, A., et al. (2019). Twenty-three Unsolved Problems in Hydrology (UPH)–a community perspective. Hydrological Sciences Journal, 64(10). https://doi.org/10.1080/02626667.2019.1620507.

Blöschl, G., Sivapalan, M., 1997. Process controls on regional flood frequency: Coefficient of variation and basin scale. Water Resour. Res. 33 (12), 2967–2980. https://doi.org/10.1029/97wr00568.

Blöschl, G., Sivapalan, M., Savenije, H., Wagener, T., Viglione, A., 2013. Runoff prediction in ungauged basins: synthesis across processes. places and scales. Cambridge University Press.

Borga, M., Boscolo, P., Zanon, F., Sangati, M., 2007. Hydrometeorological analysis of the 29 August 2003 flash flood in the Eastern Italian Alps. J. Hydrometeorol. 8 (5), 1049–1067. https://doi.org/10.1175/Jhm593.1.

Breinl, K., Müller-Thomy, H., Blöschl, G., 2020. Space-Time Characteristics of Areal Reduction Factors and Rainfall Processes. J. Hydrometeorol. 21 (4), 671–689. https://doi.org/10.1175/Jhm-D-19-0228.1.

Chiew, F.H.S., 2006. Estimation of rainfall elasticity of streamflow in Australia. Hydrological Sciences Journal-Journal Des Sciences Hydrologiques 51 (4), 613–625. https://doi.org/10.1623/hysj.51.4.613.

Costa, V., Fernandes, W., 2017. Bayesian estimation of extreme flood quantiles using a rainfall-runoff model and a stochastic daily rainfall generator. J. Hydrol. 554, 137–154. https://doi.org/10.1016/j.jhydrol.2017.09.003.

Cunderlik, J.M., Ouarda, T.B.M.J., 2006. Regional flood-duration-frequency modeling in the changing environment. J. Hydrol. 318 (1–4), 276–291. https://doi.org/10.1016/j.jhydrol.2005.06.020.

Cunderlik, J.M., Ouarda, T.B.M.J., 2007. Regional flood-rainfall duration-frequency modeling at small ungaged sites. J. Hydrol. 345 (1–2), 61–69. https://doi.org/10.1016/j.jhydrol.2007.07.011.

Dotzek, N., Groenemeijer, P., Feuerstein, B., Holzer, A.M., 2009. Overview of ESSL's severe convective storms research using the European Severe Weather Database ESWD. Atmos. Res. 93 (1–3), 575–586. https://doi.org/10.1016/j.atmosres.2008.10.020.

Duethmann, D., Blöschl, G., Parajka, J., 2020. Why does a conceptual hydrological model fail to correctly predict discharge changes in response to climate change? Hydrol. Earth Syst. Sci. 24 (7), 3493–3511. https://doi.org/10.5194/hess-24-3493-2020.

O.J. Dunn 6 3 1964 241 252.

Franchini, M., Galeati, G., Lolli, M., 2005. Analytical derivation of the flood frequency curve through partial duration series analysis and a probabilistic representation of the runoff coefficient. J. Hydrol. 303 (1–4), 1–15. https://doi.org/10.1016/j.jhydrol.2004.07.008.

Fürst, J. (2003). Fliessgewässer und Seen. Karte 1.2, Hydrologischer Atlas Österreich. Österreichischer Kunst und Kulturverlag und Bundesministerium für Land-und Forstwirtschaft. Umwelt und Wasserwirtschaft, Wien.

Gaál, L., Szolgay, J., Kohnová, S., Parajka, J., Merz, R., Viglione, A., Blöschl, G., 2012. Flood timescales: Understanding the interplay of climate and catchment processes through comparative hydrology. Water Resour. Res. 48 (4) https://doi.org/10.1029/2011WR011509.

Gao, C., Booij, M.J., Xu, Y.-P., 2020. Development and hydrometeorological evaluation of a new stochastic daily rainfall model: Coupling Markov chain with rainfall event model. J. Hydrol. 589, 125337. https://doi.org/10.1016/j.jhydrol.2020.125337.

Goel, N.K., Kurothe, R.S., Mathur, B.S., Vogel, R.M., 2000. A derived flood frequency distribution for correlated rainfall intensity and duration. J. Hydrol. 228 (1–2), 56–67. https://doi.org/10.1016/S0022-1694(00)00145-1.

Guillot, P., 1993. The Arguments of the Gradex Method - a Logical Support to Assess Extreme Floods. Extreme Hydrological Events: Precipitation, Floods and Droughts (213), 287–298.

Guo, J.L., Li, H.Y., Leung, L.R., Guo, S.L., Liu, P., Sivapalan, M., 2014. Links between flood frequency and annual water balance behaviors: A basis for similarity and regionalization. Water Resour. Res. 50 (2), 937–953. https://doi.org/10.1002/2013wr014374.

Gutknecht, D., Reszler, C., Blöschl, G., 2002. Das Katastrophenhochwasser vom 7. August 2002 am Kamp—Eine erste Einschätzung. Elektrotechnik und Informationstechnik 119 (12), 411–413.

Hashemi, A.M., Franchini, M., O'Connell, P.E., 2000. Climatic and basin factors affecting the flood frequency curve: PART I-A simple sensitivity analysis based on the continuous simulation approach. Hydrol. Earth Syst. Sci. 4 (3), 463–482. https://doi.org/10.5194/hess-4-463-2000.

Hengl, T., Mendes de Jesus, J., Heuvelink, G.B.M., Ruiperez Gonzalez, M., Kilibarda, M., Blagotić, A., Shangguan, W., Wright, M.N., Geng, X., Bauer-Marschallinger, B., Guevara, M.A., Vargas, R., MacMillan, R.A., Batjes, N.H., Leenaars, J.G.B., Ribeiro, E., Wheeler, I., Mantel, S., Kempen, B., Bond-Lamberty, B., 2017. SoilGrids250m: Global gridded soil information based on machine learning. PLoS ONE 12 (2), e0169748. https://doi.org/10.1371/journal.pone.0169748.

Holko, L., Parajka, J., Kostka, Z., Skoda, P., Blöschl, G., 2011. Flashiness of mountain streams in Slovakia and Austria. J. Hydrol. 405 (3–4), 392–401. https://doi.org/10.1016/j.jhydrol.2011.05.038.
IUSS Working Group WRB. (2015). World reference base for soil resources 2014, update 2015: International soil classification system for naming soils and creating legends for soil maps. World Soil Resources Reports No. 106. FAO, Rome. 192 pp.
Javelle, P., Ouarda, T.B.M.J., Bobée, B., 2003. Spring flood analysis using the flood-duration-frequency approach: application to the provinces of Quebec and Ontario. Canada. Hydrological Processes 17 (18), 3717–3736. https://doi.org/10.1002/(ISSN)1099-108510.1002/hyp.v17:1810.1002/hyp.1349.
Javelle, P., Ouarda, T.B.M.J., Lang, M., Bobée, B., Galéa, G., Grésillon, J.M., 2002. Development of regional flood-duration–frequency curves based on the index-flood method. J. Hydrol. 258 (1–4), 249–259. https://doi.org/10.1016/S0022-1694(01)00577-7.
Keefer, T.O., Renard, K.G., Goodrich, D.C., Heilman, P., Unkrich, C., 2016. Quantifying Extreme Rainfall Events and Their Hydrologic Response in Southeastern Arizona. J. Hydrol. Eng. 21 (1), 04015054. https://doi.org/10.1061/(ASCE)HE.1943-5584.0001270.
Kiem, A.S., Franks, S.W., Kuczera, G., 2003. Multi-decadal variability of flood risk. Geophys. Res. Lett. 30 (2) https://doi.org/10.1029/2002gl015992.
Klein, B., Pahlow, M., Hundecha, Y., Schumann, A., 2010. Probability Analysis of Hydrological Loads for the Design of Flood Control Systems Using Copulas. J. Hydrol. Eng. 15 (5), 360–369. https://doi.org/10.1061/(Asce)He.1943-5584.0000204.
Komma, J., Reszler, C., Blöschl, G., Haiden, T., 2007. Ensemble prediction of floods - catchment non-linearity and forecast probabilities. Nat. Hazards Earth Syst. Sci. 7 (4), 431–444. https://doi.org/10.5194/nhess-7-431-2007.
Koutsoyiannis, D., Kozonis, D., Manetas, A., 1998. A mathematical framework for studying rainfall intensity-duration-frequency relationships. J. Hydrol. 206 (1–2), 118–135. https://doi.org/10.1016/S0022-1694(98)00097-3.
W.H. Kruskal W.A. Wallis 47 260 1952 583 621.
Li, Z.W., Xu, X.L., Xu, C.H., Liu, M.X., Wang, K.L., Yu, B.F., 2017. Annual Runoff is Highly Linked to Precipitation Extremes in Karst Catchments of Southwest China. J. Hydrometeorol. 18 (10), 2745–2759. https://doi.org/10.1175/Jhm-D-17-0032.1.
Llasat, M.C., 2001. An objective classification of rainfall events on the basis of their convective features: Application to rainfall intensity in the northeast of Spain. Int. J. Climatol. 21 (11), 1385–1400. https://doi.org/10.1002/joc.692.
D. Lun S. Fischer A. Viglione G. Blöschl Detecting flood-rich and flood-poor periods in annual peak discharges across Europe Water Resources Research 56 7 2020 e2019WR026575 10.1029/2019WR026575.
Matulla, C., Penlap, E.K., Haas, P., Formayer, H., 2003. Comparative analysis of spatial and seasonal variability: Austrian precipitation during the 20th century. Int. J. Climatol. 23 (13), 1577–1588. https://doi.org/10.1002/(ISSN)1097-008810.1002/joc.v23:1310.1002/joc.960.
McDonnell, J.J., 2013. Are all runoff processes the same? Hydrol. Process. 27 (26), 4103–4111. https://doi.org/10.1002/hyp.v27.2610.1002/hyp.10076.
Merz, R., Blöschl, G., 2003. A process typology of regional floods. Water Resour. Res. 39 (12) https://doi.org/10.1029/2002wr001952.
Merz, R., Blöschl, G., Parajka, J., 2006. Spatio-temporal variability of event runoff coefficients. J. Hydrol. 331 (3–4), 591–604. https://doi.org/10.1016/j.jhydrol.2006.06.008.
Merz, R., Blöschl, G., 2008. Flood frequency hydrology: 2. Combining data evidence. Water Resour. Res. 44 (8) https://doi.org/10.1029/2007wr006745.
Merz, R., Blöschl, G., 2009a. Process controls on the statistical flood moments - a data based analysis. Hydrol. Process. 23 (5), 675–696. https://doi.org/10.1002/hyp.v23:510.1002/hyp.7168.
Merz, R., Blöschl, G., 2009b. A regional analysis of event runoff coefficients with respect to climate and catchment characteristics in Austria. Water Resour. Res. 45 (1) https://doi.org/10.1029/2008WR007163.
Mohymont, B., Demaree, G.R., Faka, D.N., 2004. Establishment of IDF-curves for precipitation in the tropical area of Central Africa - comparison of techniques and results. Nat. Hazards Earth Syst. Sci. 4 (3), 375–387. https://doi.org/10.5194/nhess-4-375-2004.
Müller-Thomy, H., Sikorska, A.E., 2019. Does the complexity in temporal precipitation disaggregation matter for a lumped hydrological model? Hydrological Sciences Journal-Journal Des Sciences Hydrologiques 64 (12), 1453–1471. https://doi.org/10.1080/02626667.2019.1638926.
Naghettini, M., Potter, K.W., Illangasekare, T., 1996. Estimating the upper tail of flood-peak frequency distributions using hydrometeorological information. Water Resour. Res. 32 (6), 1729–1740. https://doi.org/10.1029/96wr00200.
Norbiato, D., Borga, M., Esposti, S.D., Gaume, E., Anquetin, S., 2008. Flash flood warning based on rainfall thresholds and soil moisture conditions: An assessment for gauged and ungauged basins. J. Hydrol. 362 (3–4), 274–290. https://doi.org/10.1016/j.jhydrol.2008.08.023.
Okoli, K., Mazzolenni, M., Breinl, K., Di Baldassarre, G., 2019. A systematic comparison of statistical and hydrological methods for design flood estimation. Hydrol. Res. 50 (6), 1665–1678. https://doi.org/10.2166/nh.2019.188.
Österreichische Bodenkundliche Gesellschaft Bodenaufnahmesysteme in Österreich Vol. 62 2001 Vienna.
Packman, J.C., Kidd, C.H.R., 1980. A Logical Approach to the Design Storm Concept. Water Resour. Res. 16 (6), 994–1000. https://doi.org/10.1029/WR016i006p00994.
Panthou, G., Vischel, T., Lebel, T., Quantin, G., Molinie, G., 2014. Characterising the space-time structure of rainfall in the Sahel with a view to estimating IDAF curves. Hydrol. Earth Syst. Sci. 18 (12), 5093–5107. https://doi.org/10.5194/hess-18-5093-2014.
Paquet, E., Garavaglia, F., Garcon, R., Gailhard, J., 2013. The SCHADEX method: A semi-continuous rainfall-runoff simulation for extreme flood estimation. J. Hydrol. 495, 23–37. https://doi.org/10.1016/j.jhydrol.2013.04.045.
Parajka, J., Merz, R., Blöschl, G., 2005. Regionale Wasserbilanzkomponenten für Österreich auf TagesbasisRegional Water Balance components in Austria on a daily basis. Österreichische Wasser-und Abfallwirtschaft 57 (3-4), 43–56.
Parrett, C. (1997). Regional analysis of annual precipitation maxima in Montana (Vol. 97): US Department of the Interior, US Geological Survey.
Pebesma, E.J., Wesseling, C.G., 1998. Gstat: A program for geostatistical modelling, prediction and simulation. Comput. Geosci. 24 (1), 17–31. https://doi.org/10.1016/S0098-3004(97)00082-4.
Perdigão, R.A.P., Blöschl, G., 2014. Spatiotemporal flood sensitivity to annual precipitation: Evidence for landscape-climate coevolution. Water Resour. Res. 50 (7), 5492–5509. https://doi.org/10.1002/wrcr.v50.710.1002/2014WR015365.
Pilgrim, D.H., Cordery, I., 1975. Rainfall Temporal Patterns for Design Floods. Journal of the Hydraulics Division-Asce 101 (1), 81–95.
Piper, D., Kunz, M., Ehmele, F., Mohr, S., Muhr, B., Kron, A., Daniell, J., 2016. Exceptional sequence of severe thunderstorms and related flash floods in May and June 2016 in Germany - Part 1: Meteorological background. Nat. Hazards Earth Syst. Sci. 16 (12), 2835–2850. https://doi.org/10.5194/nhess-16-2835-2016.
Powell, M. J. D. (2009). The BOBYQA algorithm for bound constrained optimization without derivatives. Cambridge NA Report NA2009/06, University of Cambridge, Cambridge, 26-46.
Rahman, A., Weinmann, P.E., Hoang, T.M.T., Laurenson, E.M., 2002. Monte Carlo simulation of flood frequency curves from rainfall. J. Hydrol. 256 (3–4), 196–210. https://doi.org/10.1016/S0022-1694(01)00533-9.
Rieger, W., 1999. Topographischer feuchteindex für ganz Österreich. Angewandte geographische Informationsverarbeitung 11, 436–447.
Rogger, M., Pirkl, H., Viglione, A., Komma, J., Kohl, B., Kirnbauer, R., Merz, R., Blöschl, G., 2012. Step changes in the flood frequency curve: Process controls. Water Resour. Res. 48 (5) https://doi.org/10.1029/2011WR011187.
Sane, Y., Panthou, G., Bodian, A., Vischel, T., Lebel, T., Dacosta, H., Quantin, G., Wilcox, C., Ndiaye, O., Diongue-Niang, A., Diop Kane, M., 2018. Intensity-duration-frequency (IDF) rainfall curves in Senegal. Nat. Hazards Earth Syst. Sci. 18 (7), 1849–1866. https://doi.org/10.5194/nhess-18-1849-2018.
Sankarasubramanian, A., Vogel, R.M., Limbrunner, J.F., 2001. Climate elasticity of streamflow in the United States. Water Resour. Res. 37 (6), 1771–1781. https://doi.org/10.1029/2000wr900330.
Schaefer, M.G., 1990. Regional Analyses of Precipitation Annual Maxima in Washington State. Water Resour. Res. 26 (1), 119–131. https://doi.org/10.1029/89wr01513.
Seibert, P., Frank, A., Formayer, H., 2007. Synoptic and regional patterns of heavy precipitation in Austria. Theor. Appl. Climatol. 87 (1–4), 139–153. https://doi.org/10.1007/s00704-006-0198-8.
Sivapalan, M., Blöschl, G., 1998. Transformation of point rainfall to areal rainfall: Intensity-duration frequency curves. J. Hydrol. 204 (1–4), 150–167. https://doi.org/10.1016/S0022-1694(97)00117-0.
Sivapalan, M., Blöschl, G., Merz, R., Gutknecht, D., 2005. Linking flood frequency to long-term water balance: Incorporating effects of seasonality. Water Resour. Res. 41 (6) https://doi.org/10.1029/2004wr003439.
Slater, L.J., Villarini, G., 2016. Recent trends in US flood risk. Geophys. Res. Lett. 43 (24), 12428–12436. https://doi.org/10.1002/2016gl071199.
Smith, J.A., 1992. Representation of Basin Scale in Flood Peak Distributions. Water Resour. Res. 28 (11), 2993–2999. https://doi.org/10.1029/92wr01718.
Smith, J.A., Villarini, G., Baeck, M.L., 2011. Mixture Distributions and the Hydroclimatology of Extreme Rainfall and Flooding in the Eastern United States. J. Hydrometeorol. 12 (2), 294–309. https://doi.org/10.1175/2010jhm1242.1.
Stein, L., Clark, M. P., Knoben, W. J. M., Pianosi, F., & Woods, R. (2021). How do climate and catchment attributes influence flood generating processes? A large-sample study for 671 catchments across the contiguous USA. Water Resources Research, (published online). https://doi.org/10.1029/2020WR028300.
Struthers, I., Sivapalan, M., 2007. A conceptual investigation of process controls upon flood frequency: role of thresholds. Hydrol. Earth Syst. Sci. 11 (4), 1405–1416. https://doi.org/10.5194/hess-11-1405-2007.
Tang, Y., Tang, Q.H., Wang, Z.G., Chiew, F.H.S., Zhang, X.J., Xiao, H., 2019. Different Precipitation Elasticity of Runoff for Precipitation Increase and Decrease at Watershed Scale. Journal of Geophysical Research-Atmospheres 124 (22), 11932–11943. https://doi.org/10.1029/2018jd030129.
Tucker, G.E., Bras, R.L., 2000. A stochastic approach to modeling the role of rainfall variability in drainage basin evolution. Water Resour. Res. 36 (7), 1953–1964. https://doi.org/10.1029/2000wr900065.
U. S. Weather Bureau. (1958). Rainfall intensity-frequency regime, Part 2—Southeastern United States. Tech. Paper No. 29, U. S. Dept. of Commerce, Washington, D.C.
Viglione, A., Blöschl, G., 2009. On the role of storm duration in the mapping of rainfall to flood return periods. Hydrol. Earth Syst. Sci. 13 (2), 205–216. https://doi.org/10.5194/hess-13-205-2009.
Viglione, A., Merz, R., Blöschl, G., 2009. On the role of the runoff coefficient in the mapping of rainfall to flood return periods. Hydrol. Earth Syst. Sci. 13 (5), 577–593. https://doi.org/10.5194/hess-13-577-2009.
Viglione, A., Merz, R., Salinas, J.L., Bloschl, G., 2013. Flood frequency hydrology: 3. A Bayesian analysis. Water Resources Research 49 (2), 675–692. https://doi.org/10.1029/2011wr010782.
Villarini, G., Smith, J.A., 2010. Flood peak distributions for the eastern United States. Water Resour. Res. 46 (6) https://doi.org/10.1029/2009WR008395.
Vivoni, E. R., Entekhabi, D., Bras, R. L., & Ivanov, V. Y. (2007). Controls on runoff generation and scale-dependence in a distributed hydrologic model. Hydrology and

Earth System Sciences, 11(5), 1683-1701. https://doi.org/DOI 10.5194/hess-11-1683-2007.

Weber, L., Schedl, A., Lipiarski, P., 2019. IRIS Online (Interaktives Rohstoff Informations System), ein Beispiel für ein weltweit einzigartiges digitales Rohstoff-Informationssystem. BHM Berg-und Hüttenmännische Monatshefte 164 (2), 56–66.

Yang, H., Yang, D., 2011. Derivation of climate elasticity of runoff to assess the effects of climate change on annual runoff. Water Resour. Res. 47 (7) https://doi.org/10.1029/2010WR009287.

Zehe, E., Sivapalan, M., 2009. Threshold behaviour in hydrological systems as (human) geo-ecosystems: manifestations, controls, implications. Hydrol. Earth Syst. Sci. 13 (7), 1273–1297. https://doi.org/10.5194/hess-13-1273-2009.

Zhu, Z.H., Wright, D.B., Yu, G., 2018. The Impact of Rainfall Space-Time Structure in Flood Frequency Analysis. Water Resour. Res. 54 (11), 8983–8998. https://doi.org/10.1029/2018wr023550.